



Fakultät für Medizin

Klinik für Herz- und Kreislauferkrankungen des Deutschen Herzzentrums München
des Freistaates Bayern

Klinik an der Technischen Universität München

(Direktor: Prof. Dr. med. H. Schunkert)

**Assessment of the endothelium in the genesis of neoatherosclerosis
in an atherosclerotic rabbit model and in primary human cell lines**

Magdalena Annemarie Stöger

Vollständiger Abdruck der von der Fakultät für Medizin
der Technischen Universität München zur Erlangung
des akademischen Grades eines

Doktors der Medizin (Dr.med.)

genehmigten Dissertation.

Vorsitzende: Prof. Dr. Gabriele Multhoff

Prüfende/r der Dissertation:

1. Prof. Dr. Michael Joner
2. Prof. Dr. Agnes Görlach

Die Dissertation wurde am 07.04.2021 bei der Technischen Universität München eingereicht und durch die Fakultät für Medizin am 10.08.2021 angenommen.

To my family

Table of contents

1	Introduction	1
2	Background.....	2
2.1	Anatomy and histology of coronary arteries	2
2.2	Coronary Artery Disease (CAD)	2
2.2.1	Pathogenesis.....	2
2.2.2	Symptoms.....	4
2.2.3	Therapy	4
2.3	Percutaneous coronary intervention (PCI) and coronary stents	5
2.3.1	Stent thrombosis.....	7
2.3.2	Bioresorbable scaffolds (BRS).....	8
2.4	Neoatherosclerosis.....	9
2.4.1	Neoatherosclerosis in BRS	10
2.5	Hypothesis and aim	10
3	Material and methods.....	12
3.1	In vivo model and animals	12
3.1.1	Study design	12
3.1.2	Anesthesia and preoperative preparation	14
3.1.3	Operative procedure	15
3.1.4	Post-operative management.....	16
3.1.5	Euthanasia.....	16
3.1.6	Protocol for storage	17
3.1.7	Sample preparation	18
3.1.8	Analysis of the samples	19
3.2	In vitro model.....	21
3.2.1	Cell culture.....	21
3.2.1.1	Splitting of the cells.....	22
3.2.1.2	Freezing of the cells	22
3.2.2	Preliminary experiment	23
3.2.3	Permeability assay (Transwell method).....	24
3.2.3.1	LDL standard curve and measurement	26
3.2.4	Immunostaining	27
3.3	Statistics	28
4	Results	30
4.1	In vivo model	30

4.2	In vitro experiments	32
4.2.1	Permeability assay.....	32
4.2.2	Immunostaining	36
5	Discussion.....	38
5.1	Summary of results.....	38
5.2	Choice of animal models	38
5.2.1	Rabbit model.....	38
5.3	Clinical challenges of BRS	39
5.3.1	Previous investigations on reendothelialization	40
5.3.2	Factors influencing reendothelialization.....	41
5.3.2.1	Animal model.....	41
5.3.2.2	Stent geometry and coatings	41
5.3.2.3	Backbone material	42
5.4	Effect of everolimus on the endothelium.....	43
6	Conclusion	44
7	Limitations.....	45
8	Summary.....	46
9	List of references.....	47
10	List of figures	53
11	List of tables	55
12	List of abbreviations	56
13	Attachments	58
13.1	Recording schedule for animal model	58
13.2	Documentation sheet.....	59
13.3	Score sheet	60
13.4	Intervention protocol	62
14	Note of thanks	63

1. Introduction

Cardiovascular diseases are the leading cause of death worldwide, causing more than 17 million people deaths in 2015. Approximately 42% were caused by acute coronary syndrome and 38% due to stroke (WHO 2018).

Because of the increasing incidence and the fatal consequences, cardiovascular diseases are a major topic in research throughout the last decades.

Revascularization, a therapy form of coronary artery disease, is done either by coronary artery bypass grafting (CABG) or percutaneous coronary intervention (PCI) with implantation of a metal scaffold (stent). Over the past decade, there has been an evolution of stent technology with the aim to improve long-term device performance. One recently described factor for stent failure is de-novo manifestation of atherosclerosis in the evolving neointima covering the stent, termed neoatherosclerosis. Until now, the exact pathomechanism underlying the development of neoatherosclerosis is still not completely understood.

The aim of this work is therefore to investigate the pathophysiologic pathway of neoatherosclerosis with the focus on the endothelial function, assuming that an impaired endothelial barrier plays a crucial role during development of neoatherosclerosis. For this purpose, an atherosclerotic animal model was used.

Furthermore, this study investigated the effect of everolimus (an immunosuppressant widely used as a coating of stents) on endothelial barrier function, presuming that immunosuppressants impair this barrier and foster atherosclerotic changes.

2 Background

2.1 Anatomy and histology of coronary arteries

The coronary arteries are responsible for blood supply of the heart. Histologically, coronary arteries have the same morphological features as most arteries in the human body. Their walls consist of three layers: intima, media and adventitia. The intima consists of an endothelial cell layer and extracellular matrix. The internal elastic membrane is a membrane consisting of elastic fibers localized between the intima and the media. The media consists of smooth muscle cells (SMC) and extracellular matrix and represents the broadest layer of the arterial wall. SMCs are connected via gap junctions and represent the cells that produce the extracellular matrix. The outermost layer of the vessel wall is the adventitia. It consists of fibroblasts, proteoglycans, elastic fibers and collagen fibers and embeds the vessel into its surroundings. The blood and lymph supply for the vessel is also embedded in the adventitial layer (Lüllmann-Rauch 2012).

2.2 Coronary Artery Disease (CAD)

Coronary artery disease is defined as the clinical significant manifestation of atherosclerosis in the coronary arteries resulting in insufficient supply of oxygen to the myocardium (Bundesärztekammer et al. 2016). The appearance of plaques containing lipids, smooth muscle cells, inflammatory cells, connective tissue and calcification in the intima of medium- and large-sized arteries is also known as atherosclerosis (Thanassoulis 2017). Risk factors for developing coronary artery disease are among others smoking, high blood pressure, diabetes mellitus, high blood lipids (especially LDL) and increased plasma levels of homocysteine. These factors play a crucial role in the inflammatory process and impairment of the endothelial barrier, which ultimately lead to atherosclerotic changes (Ross 1999).

2.2.1 Pathogenesis

Atherosclerotic changes arise from multifactorial endothelial injury. Ross et al first described this "Response to Injury hypothesis" in 1977, stating that damaging factors, such as biochemical, hemodynamic, metabolic, infectious and inflammatory stimuli (e.g. hyperlipidemia, homocysteine, high blood pressure) may result in an impaired

endothelial barrier function. The response to this dysfunctional endothelium, including platelets, lipoproteins, hormones and changes in smooth muscle cells, may facilitate the emergence of atherosclerotic lesions (Ross et al. 1977; Nabel 2012).

Turbulent or non-laminar blood flow (for example the branches of the arteries) leads to physiological intimal thickening of the arterial wall (Yahagi et al. 2016). These areas are also prone to hemodynamic alterations that lead to endothelial dysfunction (Thanassoulis 2017).

In contrast to a healthy endothelial layer, which prevents adhesion and blood coagulation, the damaged endothelium shows increased adhesiveness and procoagulative characteristics (Ross 1999; Otsuka et al. 2012). Monocytes and other inflammatory cells adhere to the dysfunctional endothelium and migrate into the subendothelial area where they cause a local inflammatory response and develop towards macrophages. Lipids such as LDL and VLDL pass the impaired endothelial barrier and get oxidated. Macrophages take up the oxidated lipids, transforming them into foam cells. These early atherosclerotic changes in the vessel wall are known as 'fatty streaks' or intimal xanthoma (Yahagi et al. 2016).

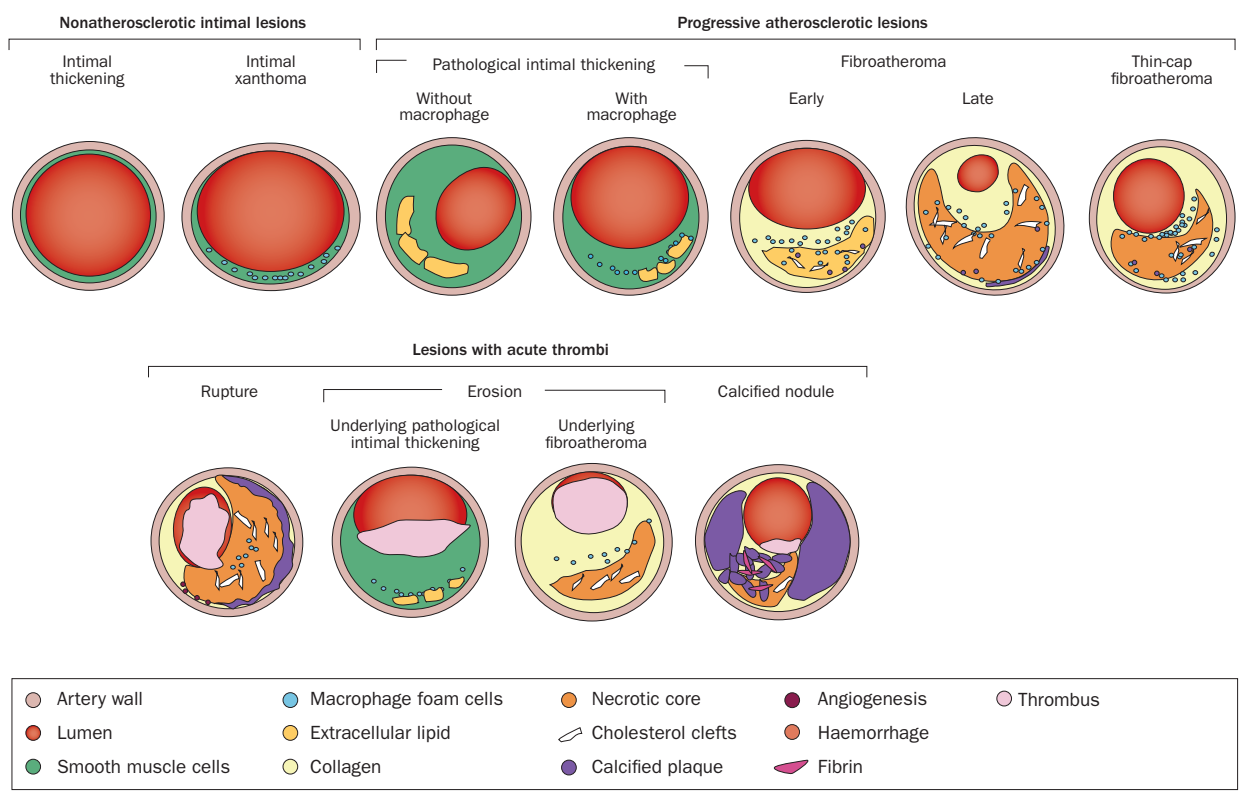


Figure 1: Classification of atherosclerotic lesions modified after Yahagi et al, 2016

Eventually, smooth muscle cells (SMC) migrate from the media into the intima. Activated macrophages and T-lymphocytes produce a variety of hydrolytic enzymes, growth factors, cytokines and chemokines, which lead to necrosis (Ross 1999). Lipid pools form, consisting of apoptotic and necrotic SMC, extracellular matrix, lipids and calcification, turning these early atherosclerotic changes into pathological intimal thickening. Finally, fibroatheroma develop with a thick fibrous cap covering the atherosclerotic lesion. Secretion of proteases result in thinning of the cap, ultimately resulting in a thin-cap fibroatheroma (TCFA). Such lesions are regarded as vulnerable plaques due to their high likelihood of rupture with subsequent arterial thrombosis. Yahagi et al describe three mechanisms that can lead to acute coronary thrombosis (=myocardial infarction). Plaque rupture is the most common cause and is most likely the endpoint of continuing cap thinning. Plaque erosion is a less common cause of thrombosis and is characterized by a damaged endothelium over a pathological intimal thickening or over a fibroatheroma causing platelets to form a thrombus. The calcified nodule is the third and least common cause and it's pathophysiology is not completely understood yet. It is found in highly calcified arteries in patients with diabetes, chronic renal failure and older patients and might possibly be the result of the erosion of small calcified nodules enclosed by fibrosis, neovascularization and inflammation (Yahagi et al. 2016; Otsuka et al. 2014).

2.2.2 Symptoms

Symptoms of myocardial ischemia include angina pectoris or dyspnea (graded by Canadian Cardiovascular Society, CCS, or New York Heart Association, NYHA). Angina pectoris manifests itself as pain, pressure or tightness in the chest, which can radiate among other into the arms or the jaw. Ischemia can also occur without clinical symptoms. In the long-term, CAD can lead to ischemic cardiomyopathy and eventually heart failure with a high mortality (depending on the severity: annual lethality 10-50%) (Herold 2018; Airhart and Murali 2017).

2.2.3 Therapy

The main therapy concepts for treatment of CAD are divided into conservative and invasive. The basis of conservative therapy is the modification of the risk factors through lifestyle changes (e.g. smoke cessation, enhance physical activity, healthy

nutrition) and optimal medical therapy (OMT). The OMT includes a standard therapy with ASS (acetylsalicylic acid) and statins as well as the optimal treatment of comorbidities, such as high blood pressure and diabetes. ASS is a thrombocyte aggregation inhibitor that prevents thrombotic events and reduces the mortality. Statins lower the lipid level and have a positive effect on plaque stability. For patients with high blood pressure and CAD a therapy with beta-blockers is recommended. These antihypertensive drugs lower the cardiac oxygen demand, reduce angina pectoris symptoms and diminish cardiovascular morbidity and lethality (Bundesärztekammer et al. 2016; Aikawa et al. 2001; Dietz and Rauch 2003; Virmani et al. 2003).

Revascularization represents the invasive therapy concept and can be achieved by percutaneous coronary intervention (PCI) or bypass-surgery. The selection of the revascularization procedure depends on different criteria, such as location and extend of the atherosclerotic lesion, age and comorbidity, and other factors (Knuuti et al. 2020).

2.3 Percutaneous coronary intervention (PCI) and coronary stents

Andreas Grüntzig established the first percutaneous coronary intervention with balloon angioplasty in 1977 (Grüntzig and Schneider 1977; Nef et al. 2018). For this purpose, a guiding catheter was introduced into the femoral artery using Seldinger technique and placed into the coronary arteries. A dilating catheter was directed over the guiding catheter to the stenotic section to dilate the narrowed artery by filling in contrast medium to a balloon on top of the catheter (Grüntzig et al. 1979). Pure balloon angioplasty however was limited by acute dissections, restenosis, and elastic recoil of the vessel making further interventions often necessary (Serruys et al. 2012; Nef et al. 2018).

In 1986, the first coronary stents (metal scaffolds) were implanted by Puel and Sigwart (Sigwart et al. 1987). They were introduced to prevent the vessel from restenosis and counteract the elastic restoring force, improving the effect of the percutaneous coronary intervention. These first coronary devices were bare metal stents (BMS) and were widely used after their introduction (Serruys et al. 2012). However, the implantation of foreign material into the artery wall led to increased neointimal thickening (neointimal

hyperplasia) eventually leading to in-stent restenosis (which occurred in about 1/3 of patents), and in-stent thrombosis, limiting the previous clinical success in the therapy of revascularization (Fishman et al. 1994; Nef et al. 2018; Serruys et al. 2012).

Drug eluting stents (DES) were introduced as an improvement of BMS technology in the late nineties to enhance the clinical outcome after stent implantation and lower the rate of device failure with regards to in-stent restenosis observed in BMS. DES are coated with a polymer, containing antiproliferative drugs, which are eluted into the arterial wall after implantation. By inhibiting smooth muscle cell proliferation and the production of extra cellular matrix after stent implantation (Inoue et al. 2011), DES have shown to reduce neointimal hyperplasia and radically decreased restenosis and early stent thrombosis (Nef et al. 2018; Byrne et al. 2015a).

Currently FDA-approved drugs used on stent coatings are sirolimus, zotarolimus and everolimus, which are all proliferation signal inhibitors. These antiproliferative drugs don't only inhibit the proliferation of smooth muscle cells but also suppress endothelial cell proliferation, preventing the formation of an intact endothelial barrier (Finn et al. 2007b).

First generation DES, who consisted of a stainless steel platform, a persistent biocompatible polymer and either sirolimus or paclitaxel as the antiproliferative drug, showed a huge improvement regarding the prevention of restenosis by inhibiting neointimal hyperplasia. However, soon after their introduction concerns arose due to a higher likelihood of late and very late stent thrombosis in DES relative to BRS (Bavry et al. 2006). The causes for this late stent thrombosis were sustained inflammation induced by the polymer and delayed arterial healing caused by the antiproliferative drugs. (details see 2.3.1, stent thrombosis) (Koppara et al. 2015; Joner et al. 2006). New DES were designed with thinner struts (nowadays approximately 80-90µm), a more compatible polymer coating and modifications of the drug dosage - reducing the number of stent thrombosis (Byrne et al. 2015a; Byrne et al. 2009; Nef et al. 2018). Despite the lower number of stent thrombosis in second generation DES it is still a cause of concern and investigation due to the high number of patient undergoing PCI and its high mortality.

2.3.1 Stent thrombosis

Stent thrombosis (ST) is categorized regarding the occurrence after stent implantation (stent thrombosis within the first 30 days = early stent thrombosis, 1-12 months = late stent thrombosis, >12 months = very late stent thrombosis). Although new DES show a low rate of definite stent thrombosis (0.43 % (Byrne et al. 2015b)) it represents a concerning problem due to its high mortality of 30-45% (Nef et al. 2018). Especially, when the PCI is carried out due to an acute event (myocardial infarction) the rate of stent thrombosis rises to 4.4% (Byrne et al. 2015b).

Causative factors can be divided into patient related (e.g. comorbidity and compliance regarding dual antiplatelet therapy), stent related (e.g. stent design, reaction to the coating), procedural related (e.g. stent underexpansion) and lesion characteristic factors (e.g. the length, the location).

The most significant risk factors for early stent thrombosis are procedural related factors, such as stent underexpansion and interruption of dual antiplatelet therapy (DAPT) (Adriaenssens et al. 2017; Byrne et al. 2015a).

The underlying mechanism of late stent thrombosis is most likely a delayed arterial healing defined by an insufficient endothelialization of the stent struts, persistent fibrin accumulation and sustained inflammatory processes in the vessel wall. In areas with partly endothelialization and much fibrin residues, there is a high risk for thrombosis that further increases in combination with other critical patient-, lesion- or stent-related factors. Delayed arterial healing is a phenomenon associated especially with first generation DES. Newer DES have reduced this problem with improvement of the strut geometry, polymer coating and reductions of drug concentrations (Holmes et al. 2010; Finn et al. 2007a; Joner et al. 2006; Byrne et al. 2015a).

VLST is presumably triggered by a combination of different mechanisms and not only by a single cause alone. Frequently found causes were malapposition, in-stent atherosclerosis (=neoatherosclerosis), uncovered struts and stent underexpansion (Taniwaki et al. 2016) .

In a recently published study from Adriaenssens et al., results from intracoronary imaging of two hundred thirty-one patients with stent thrombosis from the PRESTIGE registry (prevention of late stent thrombosis by an interdisciplinary global European effort) were presented. All the patients had a new generation DES. The most frequent

dominant findings in early ST were uncovered struts (> 60%) and underexpansion (25.5 %). Uncovered struts were also commonly found in late (33.3 %) and very late ST (20.2%). The most frequent dominant finding for VLST was neoatherosclerosis (31.3 %) (Adriaenssens et al. 2017).

2.3.2 Bioresorbable scaffolds (BRS)

With the idea to overcome the long term limitations of permanent metal stents, which lead to ongoing inflammatory processes, impeded vasomotion, late stent failures and the necessity of repeated revascularizations (2 to 3% per year) (Wykrzykowska et al. 2017), bioresorbable scaffolds were designed. The concept of the BRS consists of a bioresorbable framework, which is entirely absorbed after a period of time and averts the permanent stimulus of a foreign body (Nef et al. 2018).

Similar to DES, the bioresorbable scaffolds elute antiproliferative drugs to prevent neointimal thickening (Sotomi et al. 2017). Different backbone materials for bioresorbable scaffold are PLLA (used in the Absorb BRS from Abbott Vascular and the DESolve BRS from Elixir medical) and magnesium (used in the Magmaris BRS from Biotronik). Ideally, the lack of a durable metallic stent should diminish the trigger for thrombosis (Sotomi et al. 2017; Serruys et al. 2012).

One of the first FDA-approved devices and extensively studied was the Absorb BRS, consisting of a PLLA backbone and eluting everolimus, dissolving in approximately 3 years (Nef et al. 2018). However, the three-year follow-up of the ABSORB III trial comparing the ABSORBBS with a standard DES (XIENCE) showed a significantly higher rate of target lesion failure in the Absorb BRS group compared to the Xience DES group (13.4% of BRS patients vs 10.4% of DES patients after 3 years) (Kereiakes et al. 2017). The failures were most likely due to increased scaffold thrombosis of the ABSORB BRS. One of the reasons for the higher number of thrombosis in the ABSORB BRS may be the thicker struts of these devices (150-160 µm) that are associated with higher thrombogenicity (Pradhan et al. 2019). Another factor might be a suboptimal implantation technique of the BRS. Different studies showed that an optimal “Pre-dilation, Sizing and Post-dilation” (PSP) technique could enhance the clinical outcome after scaffold implantation (Ortega-Paz et al. 2018).

Thrombosis in early cases was most likely associated with underexpansion of the scaffold, while the leading cause of (very) late thrombosis was malapposition. This late occurring malapposition is due to scaffold discontinuity associated with backbone fractures during the degradation process. The remnant struts can poke into the lumen, causing a nidus for thrombogenicity. Other causes for very late scaffold thrombosis are in-stent atherosclerosis (= neoatherosclerosis), uncovered struts and stent underexpansion (Yamaji et al. 2017; Kraak et al. 2018).

2.4 Neoatherosclerosis

Neoatherosclerosis (NA) is described as the manifestation of atherosclerotic lesions within the neointima. It is found in DES, BMS (Otsuka et al. 2015; Yamaji et al. 2017; Byrne et al. 2015a) and seen as a progressive and unstable disease that can lead to a renewed occlusion of the stented vessel. Therefore, neoatherosclerosis is a serious complication of stent therapy. The earliest and most frequent findings of NA is neointimal infiltration with macrophages. These cells tend to form clusters near the surface and the stent struts, undergo apoptosis and develop necrotic cores that are localized mainly superficial, whereas in native artery disease, foam cells are found individually throughout the intima and the necrotic cores are localized in the deep intimal stratum (Yahagi et al. 2016).

Ongoing infiltration of macrophages lead to a thinning of the fibrous cap and can result in plaque rupture. In addition, bleedings into the plaques or fibrin deposition around the stent struts may play a role in the pathogenesis of plaque destabilization. The presence of calcification can vary from none over microcalcification up to calcified sheets and is frequently observed in long-term implant duration (Yahagi et al. 2016). While atherosclerosis in native arteries develops over decades, neoatherosclerosis only needs months up to a few years to form. Furthermore, non-progressive atherosclerotic lesions can recede in native arteries, while the same type of lesions are considered progressive lesions in neoatherosclerosis that cannot regress (Yahagi et al 2016). The underlying reason for the accelerated formation of neoatherosclerotic lesions in the stented area is not fully understood yet. Studies on autopsy samples comparing neoatherosclerosis in DES and BMS showed a higher incidence in DES (31% in DES vs 16% in BMS, $p > 0.001$) and an earlier occurrence after implantation in DES than in BMS. This led to the hypothesis that the lack of a functional endothelial coverage of

the stent struts plays a role in the genesis of neoatherosclerosis (Nakazawa et al. 2011). The antiproliferative drugs eluting from the stent struts lead to an incomplete and incompetent endothelial layer and may be responsible for the higher permeability of the endothelial layer for lipids due to their influence on the cell-cell junctions. A greater amount of LDL can pass through the deficient endothelial layer and drive the development of neoatherosclerotic lesions (Otsuka et al. 2012; Otsuka et al. 2015).

2.4.1 Neoatherosclerosis in BRS

Neoatherosclerosis represents a frequent finding in DES, leading to stent failure. With the idea that bioresorbable scaffolds degrade after time and leave behind a healed vessel without any foreign matter, the reduction of neoatherosclerotic changes was anticipated. However, the first widely investigated ABSORB BRS struggled with design and implantation constraints leading to a higher number of target lesion failure than DES and a setback for these new devices. Moreover neoatherosclerosis was also shown to be a problem in ABSORB (Yamaji et al. 2017; Moriyama et al. 2018). Studies on the new generation magnesium based BRS Magmaris showed better results. There was a lower number of target lesion failures after 24 months (5.9%) (Haude et al. 2018). For comparison, the ABSORB II study showed a target lesion failure of 7.0% after 24 months. An improved endothelialization, vessel uncaging and less inflammation compared to DES might lead to a lower rate of neoatherosclerosis.

2.5 Hypothesis and aim

In a recent work from our group, the Magmaris BRS and a DES were compared regarding the incidence of neoatherosclerosis using a neoatherosclerotic rabbit model. Both devices showed the exact same geometry and design and were implanted into the iliac arteries of New Zealand White Rabbits after endothelial denudation. The rabbits received a cholesterol diet to accelerate atherosclerotic changes. The results showed a decreased incidence of NA in BRS compared to DES, seen as a significant decrease of foam cell infiltration by histopathology and intravascular imaging. The higher occurrence of foam cells in the neointima of DES compared to BRS is possibly caused by a delayed reendothelialization in DES (Nicol et al. 2020a).

The results from this study lead to the hypothesis that a delayed endothelialization might be associated with an increased development of neoatherosclerosis. The

impaired barrier function of the endothelium might lead to a higher passage of lipoproteins and macrophages and foster neoatherosclerotic changes. Therefore, the aim of this work was to investigate the difference in reendothelialization over DES relative to BRS. For this purpose, the preceding animal model was modified and an earlier time point to investigate the vessels was selected, at which differences in endothelial development are expected (28 days after stent implantation).

Furthermore, cell culture experiments were used to examine the effects of everolimus (ERL, proliferation signal inhibitor) on the function of HUVECs (Human umbilical vein endothelial cells) and the passage of LDL through an endothelial monolayer. We hypothesized, that ERL leads to an impairment of the endothelial barrier function resulting in a higher passage of lipids and therefore facilitates the formation of atherosclerotic changes.

3 Material and methods

3.1 In vivo model and animals

For the investigation of the in-stent endothelialization 14 male New Zealand White rabbits from the provider Charles River in France were chosen. The study was performed in compliance with the EU Directive 2010/62/EU for animal experiments and the German Animal Welfare Act (2018). All procedures and animal handling were approved by the Animal Research Ethical Committee of the Government of Upper Bavaria (Munich, Germany; protocol No. ROB-55.2-2532.Vet_02-16-40).

The rabbits were held at the center for preclinical research at the Klinikum rechts der Isar under the specified conditions from the EU-guideline 2010/63 and were acclimatized to the new environment for a period of at least 7 days prior to start of the experiment. The rabbits lived in a livestock room under conventional hygiene conditions with a daily light rhythm of 12h light and 12h darkness with a twilight phase in-between. The room was air conditioned with a temperature from 18 to 21° C and humidity from 45 to 65%. The male rabbits had single cages (4200 cm² lot size) made of stainless steel with PVC insets. The cages had a second level to provide additional space to rest or hide. Animals were fed ad libitum with a commercial pelleted high-fat diet (Altr. 2023 rabbit diet modified with addition of 1% cholesterol 4mm pellets, Provider Altromin Spezialfutter GmbH & Co. KG, Lage, Germany) and received water via a nipple drinker system filled with 800 ml tap water. Hay was provided for environmental enrichment and stabilization of the physiological intestinal flora. Due to the sexual maturity of 5-6 months old rabbits, the animals were kept individually to prevent hierarchy fights. However, hearing-, viewing- and smelling contact between the animals were given throughout the whole animal trial.

3.1.1 Study design

To explore the endothelialization above the stent struts we investigated the vessels of 12+2 New Zealand White rabbits 28 days after stent implantation using en-face scanning electron microscopy.

After at least one week of acclimatization, the animals nourishment was changed to a 1% cholesterol diet (Altromin Spezialfutter GmbH, Germany) (day 0). Rabbits react sensitive to a cholesterol feed and their plasma levels of cholesterol increase rapidly, which fosters the development of atherosclerotic lesions (Fan et al. 2014). On day 7

both iliac arteries were denudated using a Fogarty catheter (3.0 x 15mm, Biotronik AG, Bülach Switzerland) and stents were implanted. One of the iliac arteries was implanted a bioresorbable scaffold (Magmaris®-BRS, Biotronik AG, Bülach, Switzerland), while the contralateral artery received a drug eluting stent (316L SS-DES, Biotronik AG, Bülach Switzerland). Both stent types had the same size (3.0 x 15mm), the same structure with a 6 crown 2 link design with 150 µm strut thickness and a PLLA coating that elutes sirolimus at a concentration of 140 µg/cm². The difference was the absorbability of the BRS. The implantation was captured with angiography. After 28 days (day 35) under the continued 1% cholesterol diet, the rabbits underwent a final angiography and were then euthanized. The vessels were explanted for the investigation with a scanning electron microscope (SEM).



Figure 2: Timeline of animal experiment

Throughout the experiment, the weight and the general condition were examined routinely three times per week. A standardized score sheet was used for these evaluations (see attachment 3). In case of conspicuities such as a weight loss (>5%), increased laboratory values or signs of pain (decreased feed reception, less activity, inertia) the examination interval was shortened depending on the assessed score. In addition, after the surgical procedure, the inspection was performed daily for one week. The focus of this examination was on operative wounds and signs of stent-associated ischemic complications on the hind limbs (e.g. blue toes, weak or stopped pulse, lameness, cold paws or edema).

The food intake and defecation were controlled every day to especially ensure the cholesterol uptake (see attachment 2). Blood samples to check the serum cholesterol value and the liver values were taken before the start of the cholesterol diet ("baseline") as well as intraoperatively under anesthesia on days 7 and 35. Parameters included small blood count, AST, ALT, gamma-GT, GLDH, serum bile acids and cholesterol. In case of any signs of abnormalities a veterinarian was consulted immediately to initiate a therapeutic strategy (e.g. assisted feeding, increasing the observation frequency,

medical therapy with antibiotics, analgesics or liquid substitution) or painless release of the animal.

Discontinuation criteria with immediate and painless euthanasia of the animal:

- No food intake for more than 3 following days
- Weight loss over 15%
- Signs of pain more than 3 days after the operation
- Intraoperative dissection of a vessel
- Postoperative circulation disorder
- Reaching discontinuation criteria according to the score sheet

3.1.2 Anesthesia and preoperative preparation

The rabbits were examined shortly before the surgical intervention to check their physical health state. Ears were smeared with local anesthetic salve (Emla®-Creme, lidocain and prilocain, AstraZeneca GmbH, Wedel) and an intravenous catheter was placed in one of the lateral auricular vein (Vasofix® Safety, 20G, B. Braun Melsungen AG, Melsungen, Germany). For pain prevention metamizole (Metapyrin® 500 mg/ml, Serumwerk Bernburg AG, Bernburg) (40mg/kg KGW) was applied intravenously (i.v.) as well as an antibiotic (Enrofloxacin 10 mg/kg KGW, Bayril 2.5% injection, Bayer GmbH) was given subcutaneously. A combination of medetomidin (0.25 mg/kg KGW, Sedator Fa. Albrecht 1mg/ml) and s-ketamin (17mg/kg KGW, Ketanest Pfizer Pharma 25mg/ml) in a mixed shot was injected intramuscularly (i.m.) to induce the anesthesia and to ensure relaxation. The rabbits breathed spontaneously. An intubation was not necessary. The rabbits were positioned in supine position on a heating mat (Beurer GmbH). A nasal sonde was placed to provide additional oxygen throughout the whole intervention. Salve (Bepanthen® eyes- and nose salve, Bayer Vital GmbH, Leverkusen) was put into the eyes to protect the cornea from drying out. The surgical field on the ventral neck was shaved carefully and disinfected several times. Intraoperative monitoring included reflex status, heart rate and peripheral arterial oxygen saturation (SpO₂) by use of a pulse oximeter. Right before the first skin cut the rabbits received fentanyl i.v. (0.005 – 0.01 mg/kg KGW, Fentadon, Albrecht GmbH) to ensure surgical tolerance. In case of any pain indication (for example a rise of the pulse or the breathing rate) within the operation, additional fentanyl boli were applied i.v. as required. At the end of the intervention, the animals received atipamezol

subcutaneously (s.c.) (Antisedan, Fa. Pfizer, 5mg/kg KGW) as an antagonist of medetomidin to prevent higher side effects of prolonged sleeping time after the anesthesia such as respiratory depression or hypothermia.

The duration of the narcosis lasted for a maximum of two hours for the whole intervention.

3.1.3 Operative procedure

Before the first cut, the rabbits were tested for the absence of pain by setting a pain provocation between the toes. Then an approximately 2 cm long incision was made lateral of the trachea to expose the superficial neck muscles and fascias. These were bluntly dissected until the deep neck muscles were reached and the fascia was divided to prepare the common carotid artery. The artery was divided from the adjoining vagus nerve and slings were installed proximal and distal of the vascular access point. The artery was incised between the slings using a microdissection scissor; a 5 French vessel sheath was introduced into the vessel and fixated (Terumo®, Fr.5, 10 cm, Terumo Corporation, Tokyo, Japan). Simultaneously the rabbits received heparin (150 IE/kg KGW, heparin-natrium Inj, 25000 IE/5ml, B.Braun GmbH) and 40 mg acetylsalicylic acid (Aspirin I.V. 500 mg, 100 mg/ml, Bayer AG) over the intravenous catheter for anticoagulation. Using the sheath, a Swan-Ganz-catheter was advanced over the aortic arch and into the abdominal aorta under x-ray control (Arrow® balloon wedge pressure catheter, 5Fr. 60 cm, Arrow International, inc.; Reading, USA). An initial angiography was performed with 5ml contrast agent (Imeron® 300M, 300 mg Iod/ml, Bracco Imaging Deutschland GmbH, 1:1 diluted with heparinized Ringer's solution). The catheter was then replaced by a guidewire (Galeo, 0.0014 inch coronary guide wire, Biotronik AG, Bülach, Schweiz), which was advanced into the first iliac artery.

A Fogarty balloon catheter (Fogarty®, 3Fr., 80 cm, Edwards Lifesciences LLC, Irvine, USA) was advanced over the guidewire until the distal end of the iliac artery and used to disrupt the endothelial monolayer (arterial denudation). The denudation took place using a Fogarty-catheter 3F with an inflation volume of 0.15 ml NaCl – contrast agent mixture (50:50). The balloon was inflated and gently pulled towards the aortic bifurcation along the length of the external and common iliac artery, followed by deflation of the balloon and re-placement at the initial inflation site. This procedure was repeated twice. Afterwards, the stent premounted on a balloon catheter was advanced

over the guidewire until a position beyond the branching of the internal iliac artery. The stent was implanted with a nominal pressure of 10 ATM for the bioresorbable scaffold and 12 ATM for the drug eluting stent using an inflator (Merit Medical Systems, Inc., South Jordan, Utah, USA). The procedure for denudation and stent implantation was then repeated in the contralateral iliac artery. A final angiography was performed to rule out dissection or aneurysm before the sheath was removed and the carotid artery ligated. Finally, the skin was sutured and the anesthesia was partial antagonized.

3.1.4 Post-operative management

After the intervention, the animals were monitored intensively for at least 2 hours and were brought back into their cages after reawakening. For analgesia the rabbits received buprenorphine (0.025-0.01 mg/kg KGW i.v. or s.c., Buprenodale multidose 0.3mg/ml, Dechra veterinary products) after stent implantation for at least 24h or longer if necessary. From day 7 (implantation) until day 35 (euthanasia and sample preparation) the rabbits received 40mg acetylsalicylic acid orally (Aspirin migraine effervescent tablet 500mg, Bayer GmbH) daily. The tablet was dissolved in tap water.

3.1.5 Euthanasia

Before euthanasia, the rabbits received the same anesthesia as described for stent implantation; however, this time, a small laparotomy was performed to achieve surgical access to the abdominal aorta and inferior vena cava. Fentanyl (0.005 – 0.01 mg/kg KGW, Fentadon®, 50 µg/ml, Eurovet animal health B.V., Bladel, Netherlands) and metamizole (40mg/kg KGW, Metapyrin® 500 mg/ml, Serumwerk Bernburg AG, Bernburg) were applied i.v. for freedom of pain throughout this final surgical intervention. The major vessels (aorta and vena cava) inside the abdominal cavity were prepared and a 5F sheath was introduced with modified Seldinger technique. A final angiography (Imeron® 300M, 300 mg Iod/ml, injection solution Iomeprol, Bracco Imaging Deutschland GmbH, 1:1 diluted with heparinized Ringer's solution) was conducted before the animals were euthanized using 300mg/kg pentobarbital i.v. (Narcoren® Pentobarbital-Natrium, Merial GmbH, Hallbergmoos).

3.1.6 Protocol for storage

After ensuring the death of the animal, the vasculature was cleaned by rinsing with isotonic NaCl over the sheath in the aorta. To fixate the tissue, 1 to 1.5l formalin (10%; formaldehyde-solution 10.0%, buffered neutrally, stabilized with methanol, Otto Fischar GmbH & Co. KG, Saarbrücken) was then infused under physiologic pressure through the sheath to achieve pressure fixation. Then, both vessels, left iliac artery (LIA) and right iliac artery (RIA), were prepared, extracted, labelled and transferred into 50 ml falcon tubes filled with formalin (3.7%; formaldehyde-solution 3.5-3.7%, buffered neutrally, stabilized with methanol, Otto Fischar GmbH & Co. KG, Saarbrücken) for 24 hours. After 24 hours of immersion fixation formalin was replaced with glycerol 50% (Pharmacy of the Klinikum rechts der Isar) and stored for 2 hours. The vessels were put into fresh glycerol 50% for another 17 hours before they spent another 6 h in glycerol 100% (Pharmacy of the Klinikum rechts der Isar). These storing steps were followed by cutting the vessels with the implanted stents lengthwise into two halves using a fine scissor (Tungsten Carbide, Fine Science Tools, Germany) followed by pinning onto styrofoam platelets. All of the vessel halves were individually labelled, put into glycerol 100% and stored at 4°C for a minimum of 6 hours and a maximum time of one week. Then they were delivered to the Max Schaldach-endowed professorship for biomedical technology (Erlangen, Germany) for taking en-face pictures with a scanning electron microscope (Zeiss scanning electron microscope-EVO MA15 microscope, Carl Zeiss, Germany).

Table 1: Storage Protocol

Substance	Duration
Formalin 10%	Until 1-1.5l are run through the sluices
Formalin 4%	24 hours
Glycerol 50%	2 hours
Glycerol 50%	17 hours
Glycerol 100%	6 hours
Cutting	
Glycerol 100% (4°C)	Min 6 hours, max one week

3.1.7 Sample preparation

Sample preparations and scanning electron microscopy were carried out at the Max Schaldach-endowed professorship for biomedical technology with the support and help of Prof. Dr. Robert Schmiedl from the department of expert future technologies – physics, future technologies & IP / vascular intervention / Biotronik SE & Co. KG.

Before proceeding with the preparation for the scanning electron microscopy, the samples needed to be washed off the glycerol. The vessel halves were transferred into 15ml falcon tubes filled with SPB 0.1M, pH 7.4 (sodium phosphate puffer, Biotronik). After 15 minutes, the buffer was replaced and repeatedly incubated for 15 minutes. Then we replaced the SPB with deionized water for another 15 min before putting the vessels carefully into a new falcon tube with deionized water for 15 minutes. This step was followed by incubating the vessel for 15 minutes with 50% EtOH, then 15 minutes with 70% EtOH and 15 minutes with 95% EtOH. After 15 minutes with 100% EtOH the samples were put into another new falcon tube and washed 3 times with 100% EtOH each for 15 minutes.

Table 2: protocol for sample preparation

Substance	Duration
SPB 0.1 M pH 7.4	15 minutes
New SPB 0.1 M pH 7.4	15 minutes
Deionized water	15 minutes
Deionized water in new falcon tube	15 minutes
50 % EtOH	15 minutes
70 % EtOH	15 minutes
95 % EtOH	15 minutes
100 % EtOH	15 minutes
3 x 15 minutes 100 % EtOH in new falcon tube	

Table 3: Material for sample preparation (all material from the chemistry lab at the Max-Schaldach-endowed professorship)

SPB 0.1M	NaH ₂ PO ₄ 19mmol=2.28g +Na ₂ HPO ₄ 81mmol=11.50g +deionized water ca. 0.9l +NaOH 0.1M to adjust the pH to 7.4
----------	---

	+deionized water 1l
EtOH 50%	Ethanol absolute (VWR) + DI water, 50:50
EtOH 70%	Ethanol absolute (VWR) + DI water, 70:30
EtOH 95%	Ethanol absolute (VWR) + DI water, 95:5
EtOH 100%	Ethanol absolute (VWR) + DI water, pure substance

After these cleaning and dehydration steps the samples were put into a critical point dryer (Leica EM CPD 030, Leica Microsystems) to remove all remaining liquid from the tissue, a step vital for ensuring high quality SEM pictures. During the procedure the samples were placed in a small chamber of the CPD and run through a series of cooling, heating and different pressure conditions. The CPD uses CO² (Kohlendioxid Linde). The dry samples were then fixed on Leit-Tabs (Leit Tabs, Plano) and pin samples plates (Stiftprobenteller, Plano) and stored in dry nitrogen.

Right before using the SEM, the vessels were coated with gold using an AGAR sputter coater (Manual Sputter Coater, Agar Scientific).

SEM analysis was conducted on a Zeiss scanning electron microscope-EVO MA 15 microscope (Carl Zeiss, Germany). For each sample, five to eight images were taken at a working distance of 4 mm and a potential of 10 kV.

3.1.8 Analysis of the samples

For image analysis Image J (downloaded application, ImageJ 1.51j8) was used. It is a public domain Java image processing program inspired by an image program of the national institutes of health and is widely used for scientific image analysis. Different areas were measured using a freehand selection tool and the endothelialized area above the struts was calculated.

In order to obtain the area of endothelialized sections of the struts of one stent, the total area of the struts was first calculated (further explanation see “total area of the struts”). Then all the good visible non-endothelialized sections over the stent struts

("non-endothelialized area") were measured and subtracted from the total area of the struts to get the endothelialized area.

"total area of the struts – non endothelialized area = endothelialized area"

Total area of all struts

Each stent has 14 struts of the same size. To get the total area of all struts of one stent, the area of one clearly visible or good comprehensible strut was measured and multiplied with 14. To receive a more reliable result, different struts of one stent were measured and the average of these measurements was used to calculate the total area of all struts.

*"average area of one strut * 14 = total area of all struts"*

Area of one strut

The area of one strut assembles the measurements of a clearly visible or good comprehensible strut in each vessel half. E.g. the area from strut number 8 from BRS half 1 of rabbit 48 was measured (see figure 3 below). Then, the area from strut number 8 from BRS half 2 of rabbit 48 was also measured (see figure 4 below) and the results summed up for the "Area of one strut" number 8.

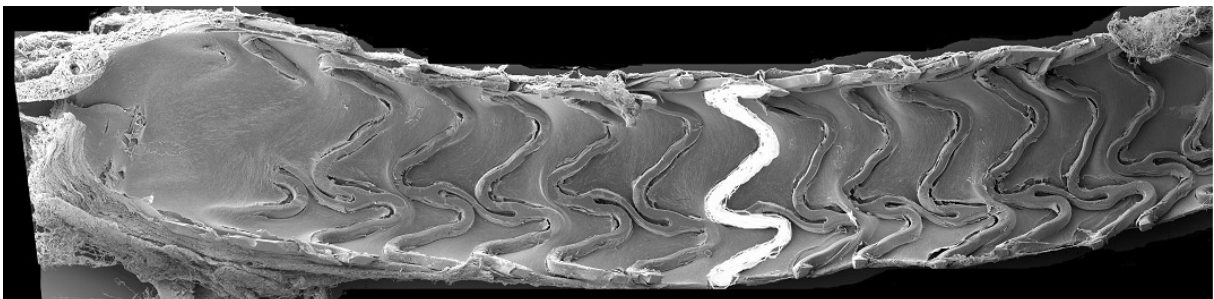


Figure 3: exemplary marking of the measured area of strut 8 (white area) in half 1 of the DES from rabbit 48, for this example the picture was edited with paint (Paint, Microsoft Windows 1903)

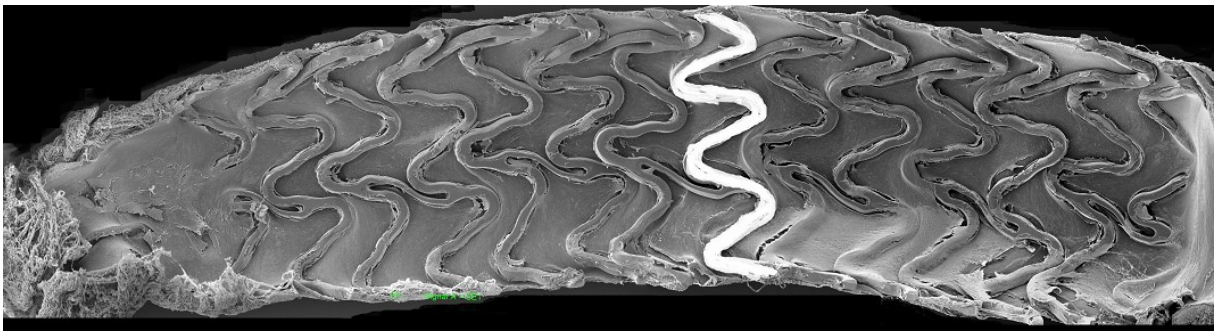


Figure 4: exemplary marking of the measured area of strut 8 (white area) in half 2 of the DES from rabbit 48, for this example the picture was edited with paint (Paint, Microsoft Windows 1903)

Non endothelialized area

In each vessel half, all of the visible and non- endothelialized areas over the struts were measured and summed up (see figure 5). The measurements from both halves were summed up to derive the non-endothelialized area of an entire stent.

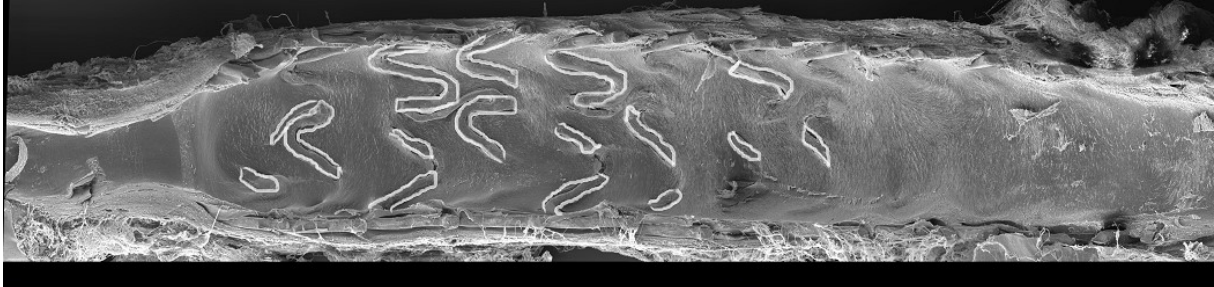


Figure 5: exemplary marking of the measured non-endothelialized areas (white edging) in BRS from rabbit 43, for this example the picture was edited with paint (Paint, Microsoft Windows 1903)

3.2 In vitro model

For the investigation of the effect of everolimus (ERL) on the endothelial cell layer and especially the cell-cell junctions, a cell culture with HUVECs (Human umbilical vein endothelial cells, Lonza, USA) was used. A permeability assay was performed to show the leakiness of the endothelium after adding ERL and immunostaining was done to visualize the influence of ERL on the cell-cell junctions with different concentrations of ERL.

3.2.1 Cell culture

Frozen HUVECs were thawed in a water bath by circling movement until there was only a small ice clot remaining. The cells were then put into a 15 ml falcon tube and 10 ml of endothelial cell growth medium (endothelial cell growth medium 2, 500ml, PromoCell) containing a supplement mix (endothelial cell growth medium 2, supplement mix for 500ml, PromoCell) was added. The suspension was centrifuged (Megafuge 1.0, Unity Lab Services) for 5 minutes with a speed of 1200 rpm and the supernatant was replaced by 10 ml fresh medium. The whole suspension was then put into a 75 ml cell culture flask to culture the cells.

Table 4: Contents of endothelial cell growth medium supplement

Contents	Final concentration after addition to medium
Fetal calf serum	0.02ml/ml
Epidermal growth factor (recombinant human)	5ng/ml
Basic fibroblast growth factor (recombinant human)	10ng/ml
Insulin-like growth factor (R3 IGF-1)	20ng/ml
Vascular endothelial growth factor 165 (recombinant human)	0.5ng/ml
Ascorbic acid	1µg/ml
Heparin	22.5µg/ml
Hydrocortisone	0.2µg/ml

3.2.1.1 Splitting of the cells

To expand the cell culture, cell culture flasks were harvested at 70%- 80% confluence. For this purpose the medium was removed from the cells and they were washed with PBS (PBS Dulbecco, w/o Ca²⁺ w/o Mg²⁺, low endotoxin, Biochrom GmBh). Thereafter the PBS was replaced with 2 ml of trypsin-EDTA (Sigma Aldrich, Germany) and the cells were incubated for 1 minute to detach them from the ground. After inspecting the flask under a microscope to ensure the cells were detached, 5 ml of medium was added to stop the reaction of the trypsin. The whole suspension was put into a 15 ml falcon tube and centrifuged for 5 minutes at a speed of 1200 rpm. The supernatant was discarded, 10 ml of fresh medium with endothelial cell growth supplement was added, and the cell pellet was diluted. Then these 10 ml of cell suspension were divided in 4 new flasks and incubated to grow. At 37° degrees a 5% CO² air atmosphere and at 100% humidity. The culture medium was changed ever 2 days.

3.2.1.2 Freezing of the cells

The cells were detached and centrifuged in the same manner as in the splitting. A new 15 ml falcon tube was prepared with 180µl DMSO (dimethyl sulfoxide 50ml, Sigma Aldrich) and 1.6ml medium. The content of the falcon tube was mixed. The supernatant

from the centrifuged cells was removed and the pellet was dissolved with the 1,8ml mixture from the other falcon tube. The whole suspension was then put into a cryotube and stored in a -80°C fridge before putting the cells in a -192°C barrel.

For the permeability assay and the staining of the cell-cell junctions and actin skeleton HUVECs between passage 5 and 7 were used.

3.2.2 Preliminary experiment

Before the actual experiment to investigate the effects of ERL on the cell-cell junctions was performed, different steps had to be assessed. The first step was to determine the needed cell concentration and incubation time to create a monolayer. For this purpose different amounts of HUVECs were seeded into a well plate, were incubated with 500µl medium and observed for 48h (set up figure 6). Cell expansion was watched after 3 hours, 24 hours and 48 hours with an Olympus microscope (BX41TF, Olympus Corporation, Tokyo, Japan) and the formation of a monolayer was evaluated to decide the adequate concentration and time periods that should be used for the experiment.

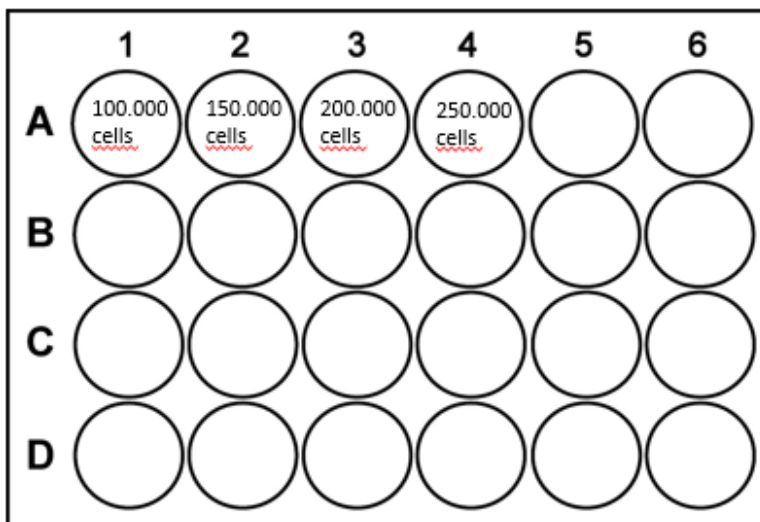


Figure 6: setup of 24 well plate for preliminary experiment

3.2.3 Permeability assay (Transwell method)

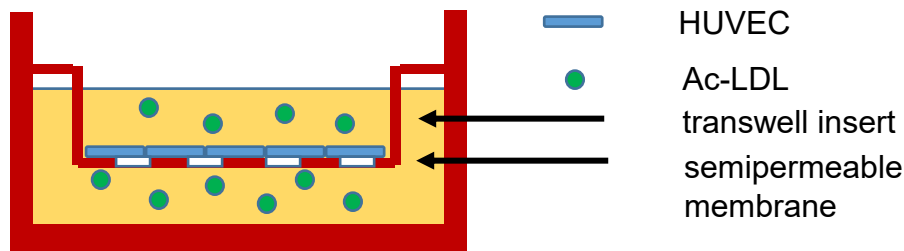


Figure 7: schematic representation transwell model

100 x 10³ cells were seeded onto each semipermeable membrane and incubated with 500µl medium in the transwell insert and 1000µl in the compartment below (12mm transwell with 0.4 µm pore polyester membrane insert, TC treated, sterile, 48/cs, Corning, Germany). They were incubated for 24 hours to form a confluent monolayer. When they reached confluency, everolimus (Everolimus, 10mg, Fluka Analytical, Sigma-Aldrich) was added in different concentrations (without ERL, 10nM, 100nM, 1µM, 10µM, 100µM). Cells were incubated with ERL for 24hours before washing the cell layer with PBS (PBS Dulbecco, w/o Ca²⁺ w/o Mg²⁺, low endotoxin, Biochrom GmbH) and adding 10µM of fluorescently labelled LDL (Alexa Fluor 488 acetylated low-density lipoprotein, invitrogen, Germany) to incubate for another 24 hours. Afterwards the supernatants from the upper and the lower chamber were put into a 96 well plate (Greiner CELLSTAR, Sigma Aldrich) and the intensity of the fluorescently marked LDL particles was measured at 490nm excitation wave length and 520nm emission wave length with a spectrophotometer (Infinite M200 Pro, Tecan, Switzerland). Additionally a standard curve was determined with known ERL and cell concentrations under identical conditions. The results were analyzed through an excel data and the LDL concentration transfer from the upper chamber to the lower chamber was calculated by using the standard curve (see figure 15: standard curve). The permeability assay was carried out three times.

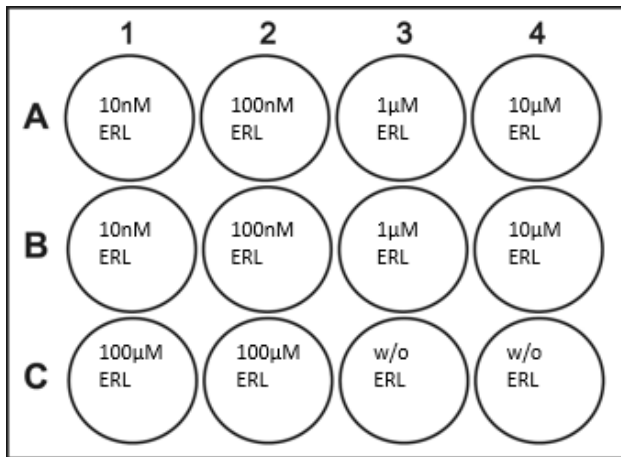


Figure 8: setup of 12 well plate with different ERL concentrations for permeability assay

Everolimus stock solution:

Table 5: ERL stock solution

1mM stock solution	1mg ERL + 1040µl DMSO
--------------------	-----------------------

Everolimus dilution:

Table 6: ERL dilution

ERL + medium	concentration
100µl ERL (1mM) + 900µl medium	100µM ERL (1000µl)
10µl ERL (1mM) + 990µl medium	10µM ERL (1000µl)
1,11µl ERL (1mM) + 1108.89µl medium	1µM ERL (1110µl)
100µl ERL (1µM) + 900µl medium	100nM (1000µl)
10µl ERL (1µM) + 990µl medium	10nM (1000µl)

LDL dilution:

Table 7: LDL dilution

60µl LDL (1mM) + 5940µl medium	10µM LDL (6000µl)
--------------------------------	-------------------

3.2.3.1 LDL standard curve and measurement

For the measurement of the LDL concentration, a standard curve was created. Therefore medium and the fluorescently labelled ac-LDL were mixed to create LDL concentrations of 5µM, 10µM and 20µM. Afterwards the dilutions were put into a 96 well plate and underwent a measurement with the spectrophotometer. The data was introduced into an excel table to create a standard curve for the calculation of the LDL concentration in the following measurement of the supernatants from the permeability assay. For the standard curve, a coordinate system was used with the known concentrations plotted on the x-axis and the measured results on the y-axis. The function for the standard curve was then created. The same measurement was then performed with the samples from the permeability assay with unknown concentration. The measurements represented the y-value and the corresponding x-value, the concentration, could be calculated using the formula from the standard curve.

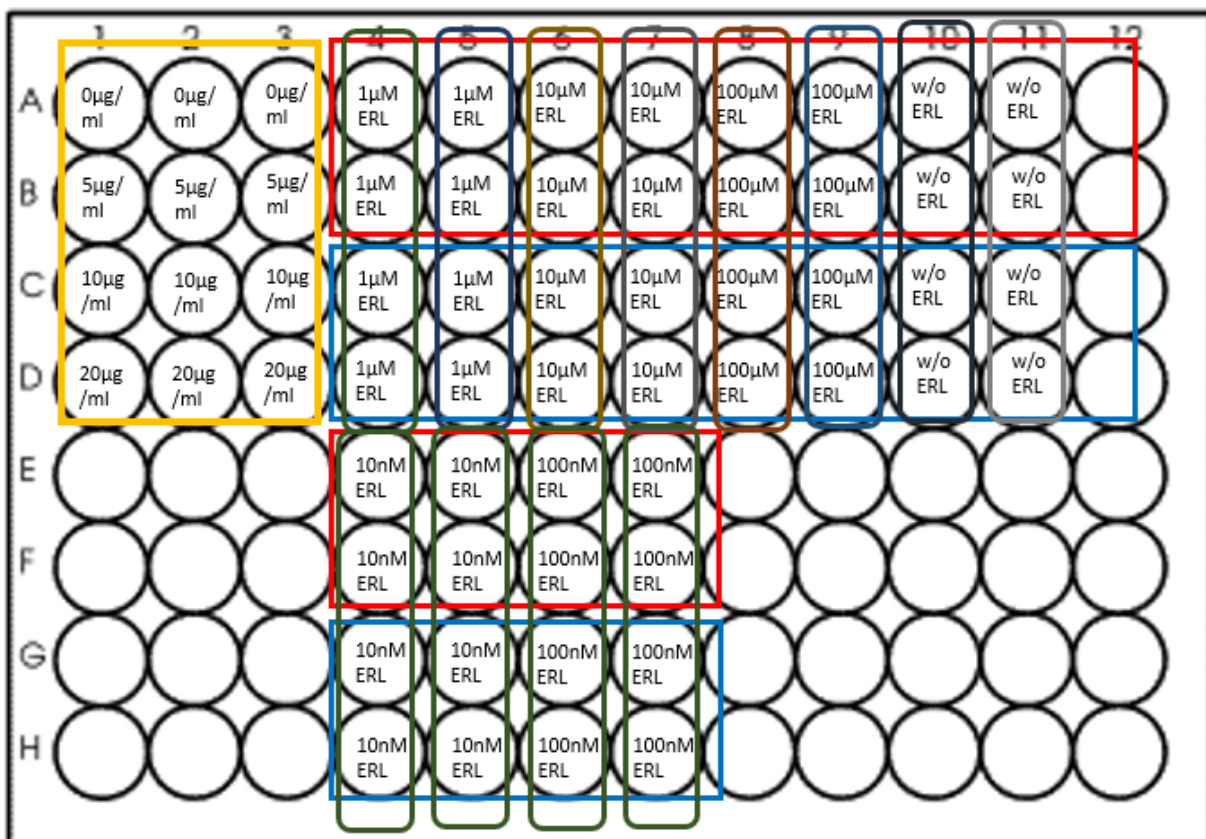


Figure 9: 96 well plate for spectrophotometer analysis, yellow framed: known ac-LDL concentrations for standard curve, red framed: samples from the upper chamber of the permeability assay with ERL concentrations given, blue frame: samples from the lower chamber of the permeability assay with ERL concentrations given

The calculated concentrations were organized in an excel table to further calculate the percentage of ac-LDL that passed from the upper into the lower compartment. ((concentration in the lower compartment/total concentration in both compartment)*100).

Stock solution for the standard curve:

Table 8: LDL dilutions for standard curve

11µl LDL(1mM) + 539µl medium	550µl (20µM)
250µl LDL(20µM) + 250µl medium	500 µl (10µM)
200µl LDL(10µM) + 200µl medium	400 µl (5µM)

3.2.4 Immunostaining

To examine the effects of ERL on the cell-cell junction we used a VE-Cadherin antibody to stain the cell-cell junctions as well as a phalloidin staining to visualize the actin skeleton and a counterstaining with DAPI.

For the staining of the cells they were washed with PBS once and then fixed with ice cold acetone:methanol (1:1), 1ml/well, for 15 minutes at room temperature. Then the samples were washed 3 times with ice cold PBS, 500µl/well, before incubating them with 1% triton X-100 (Triton X-100 solution, Sigma), 500µl/well, for 15 minutes to permeabilize the cells. After the permeabilization the samples were washed again 3 times with PBS, 500µl/well, each time for 5 minutes.

1% BSA (Bovine serum albumin, Sigma), 500µl, was added to the cells to block unspecific binding of antibodies and incubated for 30 minutes.

Thereafter, the BSA was removed and the diluted primary antibody (Anti VE-cadherin antibody, Abcam), 500µl/well, was placed onto the cells (dilution 1:1000 in 1% BSA in PBS). The antibody stayed on the samples overnight at 4°C in a humidified chamber. After decanting, the cells were washed 3 times in PBS, 500µl/well, 5 minutes each and the secondary antibody (Goat anti-rabbit IgG H&L (Alexa Fluor® 488), Abcam), 500µl/well, was added in the dark (dilution 1:1000). After one hour incubation in the dark at room temperature the samples were washed 3 times with PBS, 500µl/well, and incubated for 20 minutes with phalloidin (Alexa Fluor 594 phalloidin, Thermo Fisher), 500µl/well, to stain the cytoskeleton. The samples were then washed three times with PBS, 500µl/well, and the membranes were cut out using a scalpel and put onto a

microscope slide (Adhesive slides, SuperFrost® Plus, Menzel Gläser, VWR). A drop of DAPI (Roti®-Mount FluorCare DAPI, ROTH) was put onto the membranes and a cover glass was placed above it.

The samples were stored in a fridge at 4°C until the microscopic examination and pictures were taken.

Table 9: Dilutions for immunostaining

Antibody dilution, primary and secondary (1:1000)	6.5µl antibody + 6493.5µl BSA 1% (amount for 1 experiment)
BSA dilution (1% in PBS)	1g in 100ml PBS
Triton X-100 dilution (1% in PBS)	35µl triton X-100 + 3465µl PBS (amount for 1 experiment)
Phalloidin dilution (1:40)	150µl phalloidin + 5850µl medium (amount for 1 experiment)

The pictures were taken on a fluorescence microscope (BX41TF, Olympus Corporation, Tokyo, Japan) with a microscope camera (DP74, Olympus, Tokyo, Japan). Pictures from the three different staining (DAPI, Alexa Fluor 488 and Alexa Fluor 594 phalloidin) were always taken at the exact same spot of the sample by varying the optical filter of the fluorescence microscope to enlighten the individual stain. Afterwards, the three pictures of the different staining were merged to one picture containing VE-cadherin, cytoskeleton and nucleic staining using Image J.

The analysis of the immunostaining was executed descriptively.

3.3 Statistics

The statistical analysis and evaluation was performed using JMP (Software version 13.2.1). The results of the evaluation are given in means and standard deviation.

The statistical distribution of the data sets was first examined using the Kolmogorow-Smirnow-Test. To determine the level of significance for the normally distributed data, a student t-test was used. A p-value of <0.05 was considered to be statistically significant.

To create a better understanding of the data, tables and figures were created using Microsoft Excel (Microsoft Excel 2013, 15.0.5249.1001 – 32-Bit).

The analysis of the results of the three permeability assays was executed merely descriptively based on excel tables (Microsoft Excel 2013, 15.0.5249.1001 – 32-Bit).

4 Results

Results of this work are presented, starting with the outcomes of the animal experiment. Both reserve animals were needed due to the premature death of two rabbits. Thereafter the results from in vitro experiments are shown starting with the permeability assay followed by immunostaining.

4.1 In vivo model

Due to constraints in individualized material and production of the stents only 10 of the 12 rabbits received both DES and BRS. The last two animals received BRS in both iliac arteries. During one intervention a DES was accidentally placed too high so that implantation of the following BRS placement was not possible. In the end, SEM pictures of 10 DES and 13 BRS were evaluated.

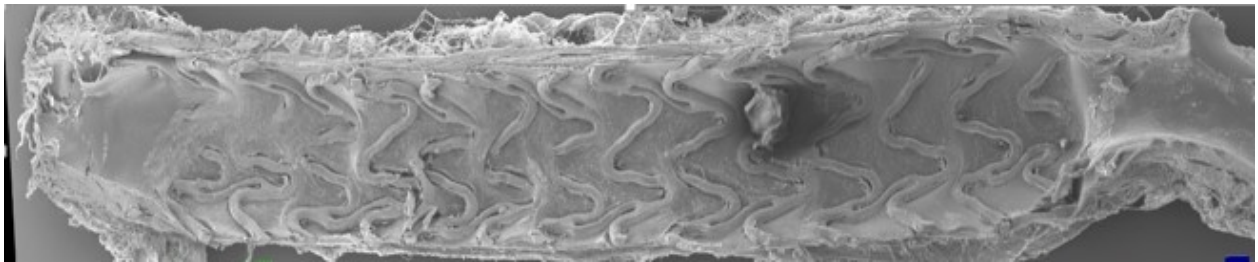


Figure 10: SEM overview of a drug eluting stent

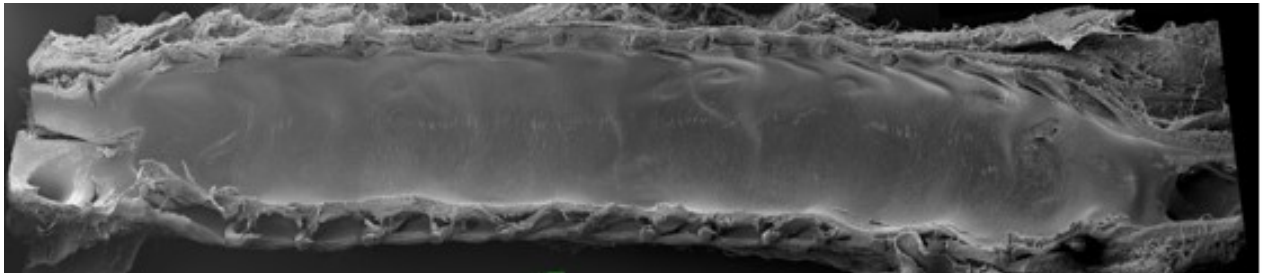


Figure 11: SEM overview of a bioresorbable scaffold

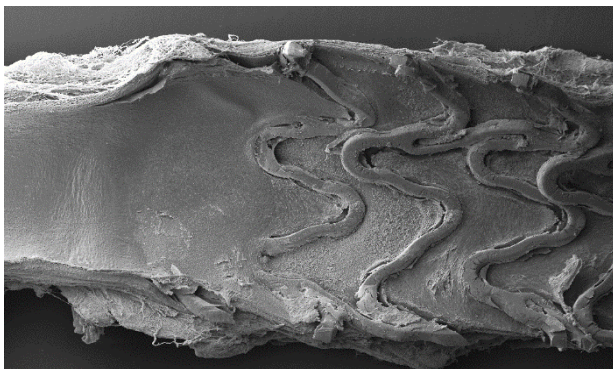


Figure 12: magnification from DES: uncovered struts

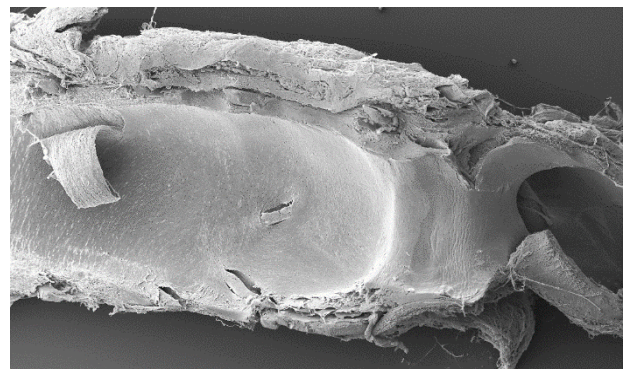


Figure 13: magnification from BRS: nearly total endothelialization

Figure 10 and 11 show the overview magnification of a SEM image from a DES (figure 10) and a BRS (figure 11). Greater degree of stent strut endothelialization of the BRS (figure 11 and 13) is clearly visible relative to the DES (figure 10 and 12). Table 10 shows the results of quantification with higher percentage of endothelialization in BRS.

Table 10: results from the analysis of the samples

		Total area of all struts	Area of one strut (average)	Endothelialized area	Non-endothelialized area	Endothelialized area %
DES	41 RIA	23.058.884.4	1.647.063.2	6.770.014.8	16.288.869.7	29.4
BRS	41 LIA	14.135.024.2	1.009.644.6	13.798.332.5	336.691.7	97.6
DES	43 RIA	25.940.183.7	1.852.870.3	8.874.031.6	17.066.152.1	34.2
BRS	43 LIA	28.123.737.1	2.008.838.4	24.451.495.6	3.672.241.5	86.9
BRS	44 RIA	27.029.039.0	1.930.645.7	26.569.636.6	459.402.4	98.3
DES	44 LIA	26.680.586.7	1.905.756.2	6.601.019.0	20.079.567.7	24.7
DES	45 RIA	27.568.877.6	1.969.205.5	6.645.870.1	20.923.007.5	24.1
BRS	45 LIA	36.508.391.8	2.607.742.3	31.707.874.1	4.800.517.7	86.9
BRS	46 RIA	24.264.672.5	1.733.190.9	23.163.498.6	1.101.173.6	95.5
DES	46 LIA	23.336.185.0	1.666.870.4	18.466.541.9	4.869.643.1	79.1
DES	47 RIA	25.217.829.7	1.801.273.6	10.891.878.1	14.325.951.6	43.2
BRS	47 LIA	21.715.358.2	1.551.097.0	18.227.855.8	3.487.502.4	83.9
BRS	48 RIA	25.362.515.5	1.811.608.3	22.255.807.1	3.106.708.4	87.8
DES	48 LIA	30.475.348.5	2.176.810.6	7.840.794.8	22.634.553.7	25.7
BRS	50 RIA	28.755.962.5	2.053.997.3	28.696.052.7	59.909.8	99.8
DES	50 LIA	29.031.901.4	2.073.707.2	10.724.060.5	18.307.840.9	36.9
DES	51 RIA	25.925.979.6	1.851.855.7	19.669.113.0	6.256.866.6	75.9
BRS	51 LIA	25.926.139.8	1.851.867.1	25.527.333.7	398.806.1	98.5
w/o	52 RIA	w/o Stent	w/o Stent	w/o Stent	w/o Stent	w/o Stent
DES	52 LIA	21.425.010.9	1.530.357.9	10.273.770.3	11.151.240.5	48.0
BRS	53 RIA	23.667.525.4	1.690.537.5	22.298.998.6	1.368.526.8	94.2
BRS	53 LIA	20.372.090.8	1.455.149.3	18.221.716.0	2.150.374.8	89.5
BRS	54 RIA	23.753.791.4	1.696.699.4	21.452.610.4	2.301.180.9	90.3
BRS	54 LIA	23.651.986.3	1.689.427.6	19.502.214.6	4.149.771.7	82.5

Units in the table are given in pixel size, one unit equalizes 3.8 μm^2

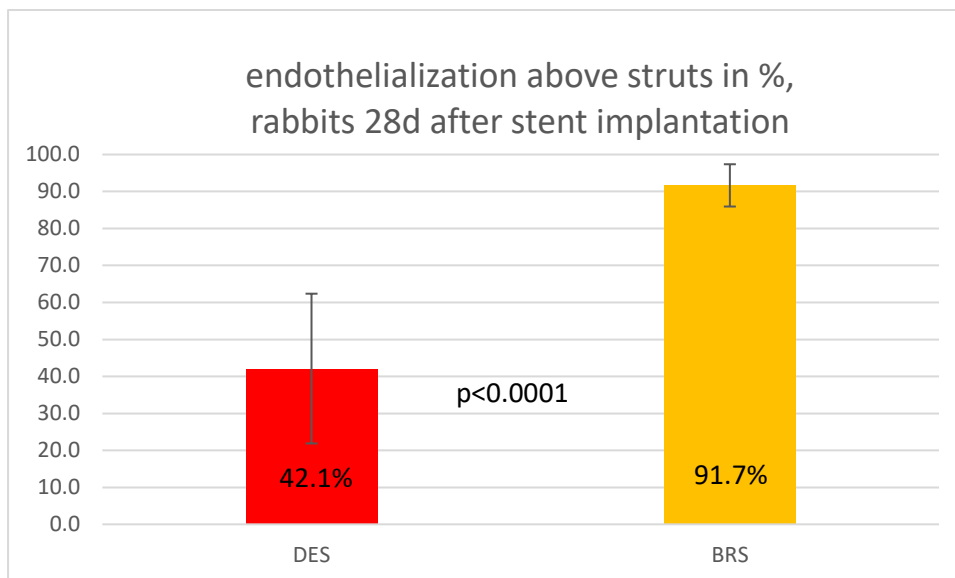


Figure 14: Endothelialization above stent struts, DES vs BRS

Quantification of stent endothelialization by analysis of the SEM pictures showed a lower percentage of endothelialization above stent struts in DES (mean: 42.1% of the total strut area were endothelialized) compared to BRS (mean: 91.7% of the total strut area) (see figure 14). This difference was statistically significant between the two groups ($p < 0.0001$ in t-test).

4.2 In vitro experiments

In the preliminary experiments, an amount of 100.000 cells per well and an incubation period of 24hours showed the best capacity to form a tight monolayer.

4.2.1 Permeability assay

The following figures and tables of the standard curve and calculation of the concentration of ac-LDL that passed through the monolayer show the results from one of the three experiments to exemplify the procedure of the evaluation (table 11-13, figure 15 and 16). Thereafter the analysis of all the experiments together ($n=3$) is shown.

Table 11 shows the standard curve for the ac-LDL concentration, necessary for calculation of the ac-LDL concentration in the transwell model. For the set-up in the transwell, see figure 9. For each concentration of ac-LDL (x-axis) three measurements with the spectrophotometer were made (y-axis). A higher concentration of ac-LDL lead

to an increased signal detected in the spectrophotometer (table 11). Mean values from these measurements are shown in table 12.

Table 11: measurements for the standard curve; X: ac-LDL concentration, Y: measurement from plate reader in fluorescent mode

Standard curve measurement	
X	Y
0	1616
0	1212
0	972
5	11565
5	12070
5	12147
10	22430
10	23431
10	21827
20	43606
20	44591
20	43010

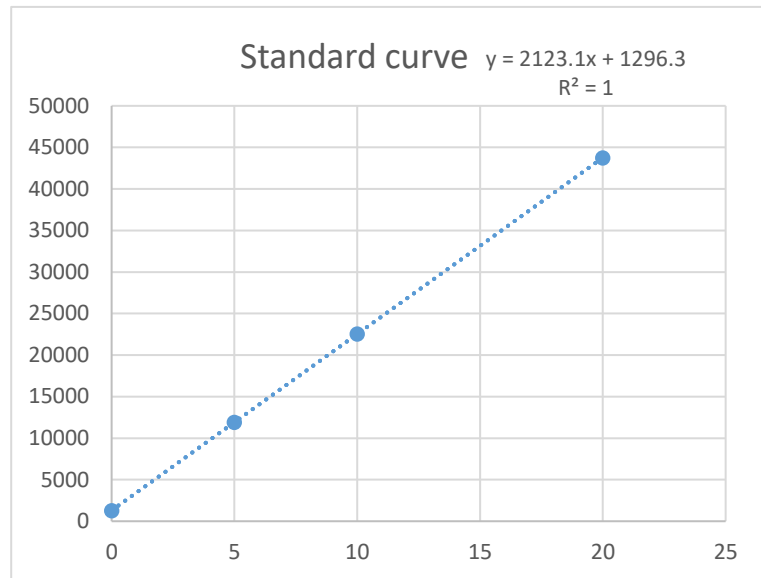


Figure 15: standard curve for LDL measurement, x-axis: ac-LDL concentration, y-axis: measurement of the plate reader in fluorescent mode

Average	
X	Y
0	1266.7 (+/-325.5)
5	11927.3 (+/-316.1)
10	22562.7 (+/-810.2)
20	43735.7 (+/-798.4)

Table 12: means of table 11 +/- standard deviation

Figure 15 shows the standard curve created with the results from table 12 – a higher fluorescent signal in connection with a higher ac-LDL concentration. The assessment of the migration from LDL from the upper to the lower compartment showed a higher/lower percentage of LDL that passed through the monolayer depending on the amount of ERL. When cells were incubated without ERL there is a lower passage of ac-LDL compared to an incubation with high concentration of ERL (9% w/o ERL vs 32% with 100µM ERL, see figure 16). Table 13 shows the results of the ac-LDL concentration calculated with the formula generated with the standard curve for the different ERL concentration. Moreover it sums up the calculation of the part of the LDL that passed through the endothelial layer. As shown in table 13, increasing concentration of everolimus (1µm to 100µm) lead to a higher passage of migrated LDL (18% to 30%).

Table 13: calculation table to evaluate the part of LDL that passed through the monolayer

ERL (μM)	LDL upper compartment (μM)		Average (μM)	Lower compartment (μM)		Average (μM)	Sum (μM)	Migrated LDL
1 μM	8.8	8.6	8.7	1.6	1.8	1.7	10.4	17%
1 μM	9.2	8.4	8.8	2.2	2.0	2.1	10.9	20%
10 μM	8.0	7.5	7.8	3.0	3.1	3.0	10.8	28%
10 μM	8.9	8.8	8.8	1.0	1.6	1.3	10.1	13%
100 μM	6.7	7.0	6.9	2.6	3.8	3.2	10.1	32%
100 μM	8.0	7.6	7.8	2.8	3.2	3.0	10.8	28%
w/o ERL	7.8	8.7	8.3	1.0	1.6	1.3	9.6	14%
w/o ERL	9.4	8.9	9.1	0.6	1.2	0.9	10.0	9%
0.1 μM	8.2	8.8	8.5	2.2	2.6	2.4	10.9	22%
0.1 μM	8.6	8.6	8.6	2.0	2.6	2.3	10.9	21%
0.01 μM	8.5	9.3	8.9	1.2	2.6	1.9	10.8	18%
0.01 μM	8.1	8.5	8.3	1.8	2.2	2.0	10.3	20%

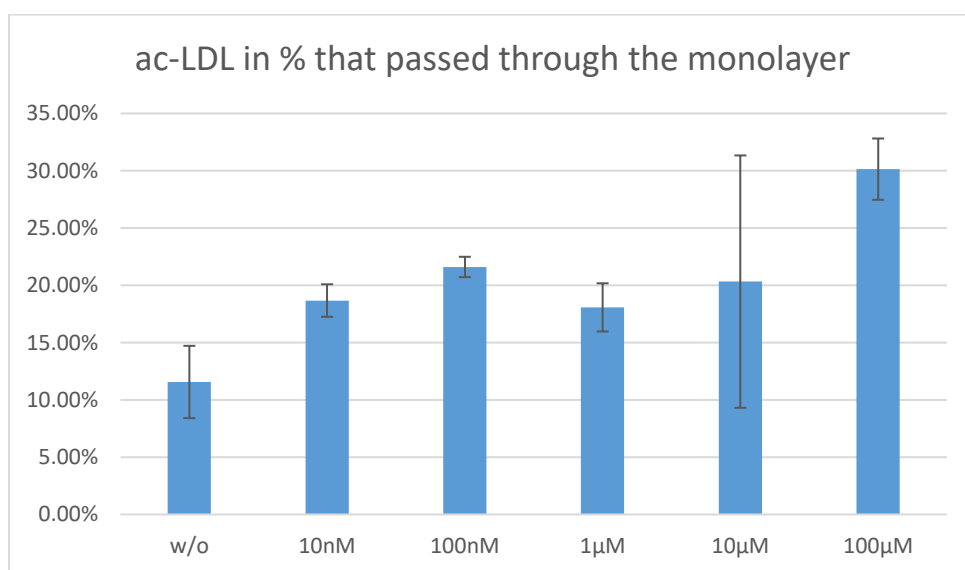


Figure 16: amount of ac-LDL that passed through the monolayer, results from one experiment

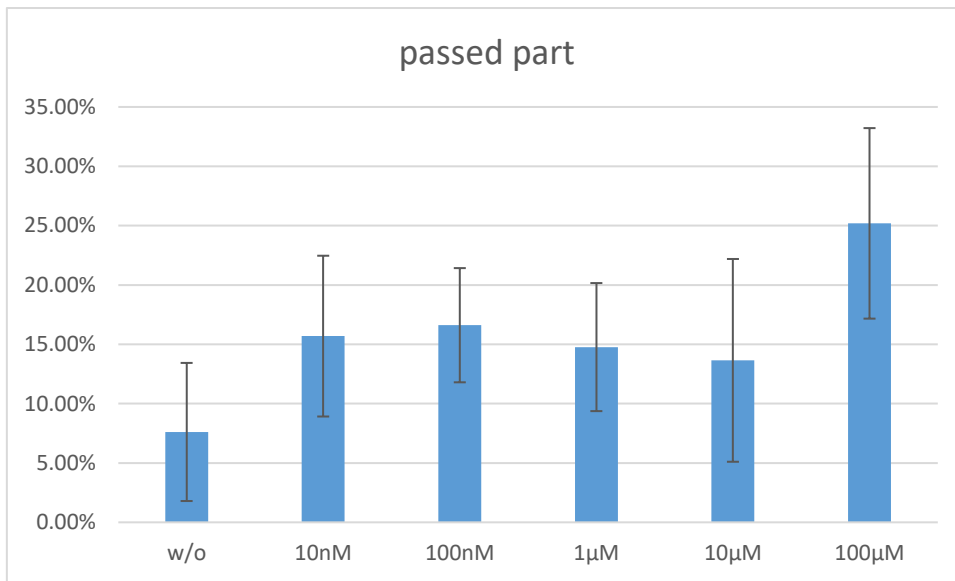


Figure 17: results n=3, Mean percentage of LDL that passed through the monolayer from all 3 experiments

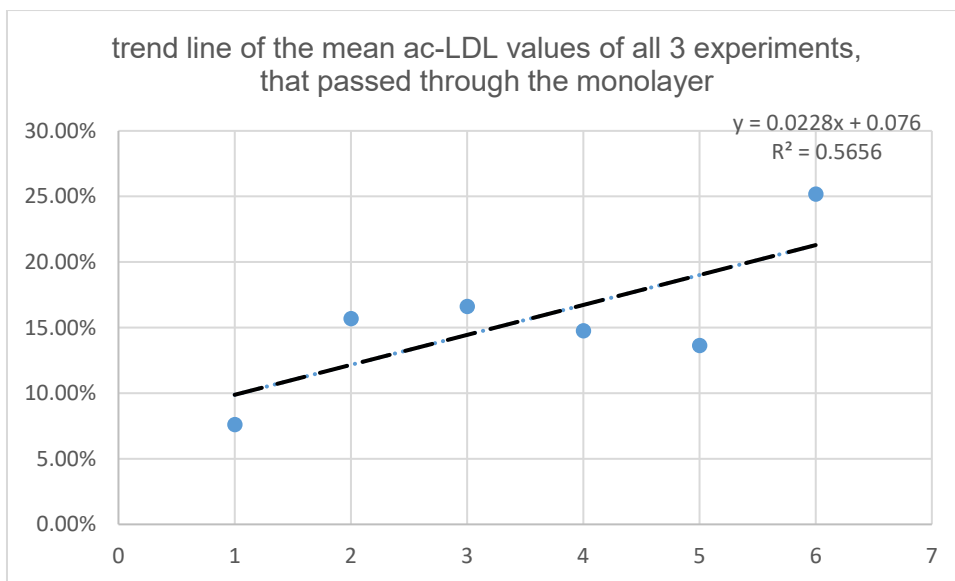


Figure 18: trend line of mean percentage of LDL that passed through the monolayer, y-axis: ERL concentration 1=w/o, 2=10nM, 3=100nM, 4=1µM, 5=10µM, 6=100µM

The permeability assay shows that the passage of ac-LDL through the monolayer was lowest in the wells without everolimus and highest in the wells with the highest concentration of ERL (figure 17). Considering the whole experiment there is a trend of an increased passage of ac-LDL in wells with a higher concentration of ERL acting on the endothelial cells (figure 18).

4.2.2 Immunostaining

The following pictures show exemplary immunostainings performed with endothelial cells from the permeability assay incubated with pure medium without ERL (figure 19-21). Cell-cell junctions were stained using a VE-cadherin antibody (figure 19). Staining of the cytoskeleton was done using phalloidin (figure 20). DAPI staining colored the cell nuclei blue (figure 21). Figure 22 to 26 show the three different stainings merged performed on cells with different ERL concentrations.

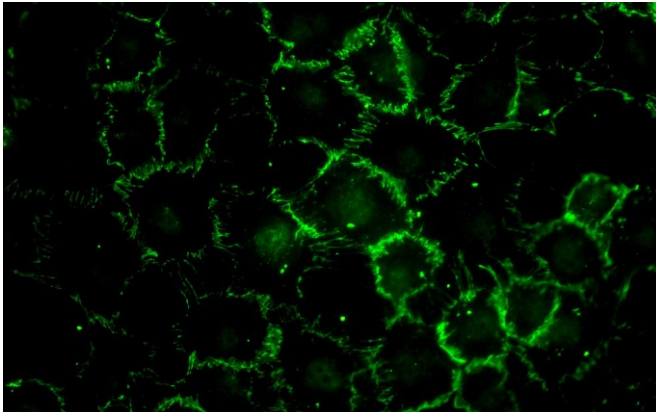


Figure 19: VE-cadherin staining of the cell-cell junctions, green

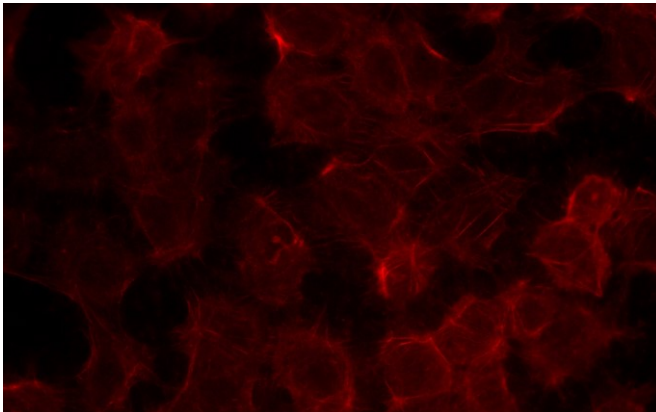


Figure 20: Phalloidin staining of cytoskeleton, red

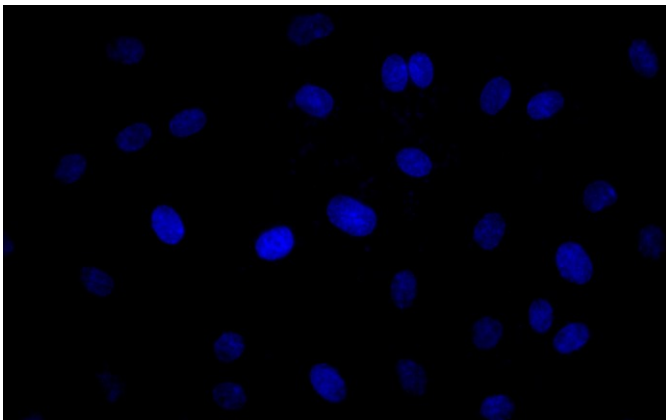


Figure 21: DAPI staining of the nucleus, blue

When cells are incubated in pure medium, well-developed cell-cell junctions can be seen (figure 22). With increasing concentration of ERL, decreased intensity of VE-Cadherin staining could be detected and the less cells in general were observable. (figure 23-27)

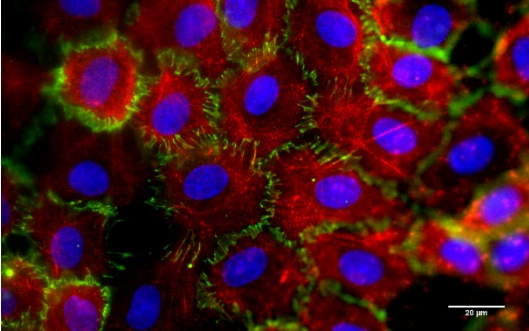


Figure 22: Immunostaining, cells w/o ERL

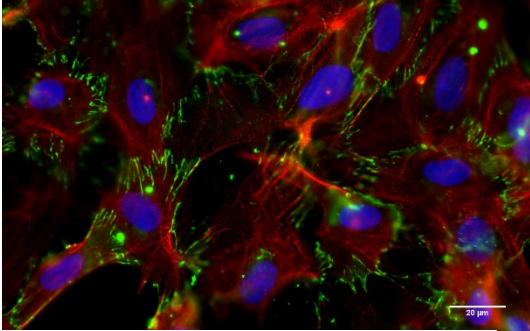


Figure 23: Immunostaining, cells with 10nM ERL

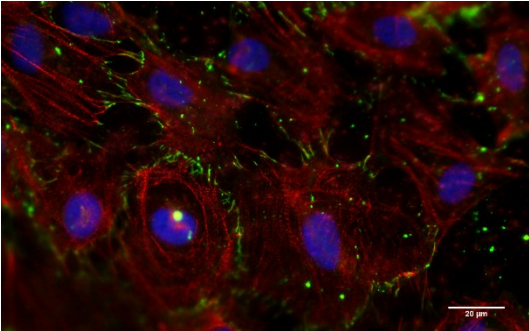


Figure 24: Immunostaining, cells with 100nM ERL

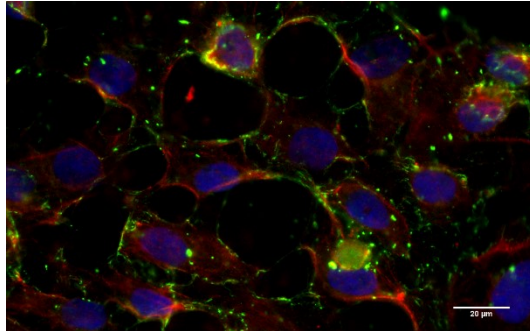


Figure 25: Immunostaining, cells with 1µM ERL

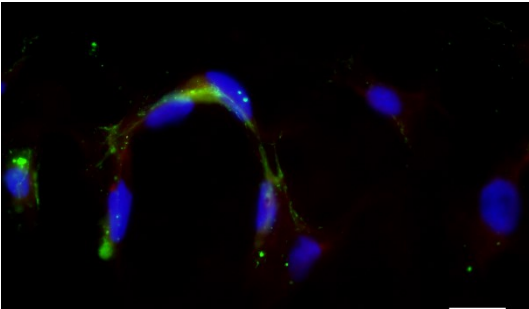


Figure 26: Immunostaining, cells with 10µM ERL

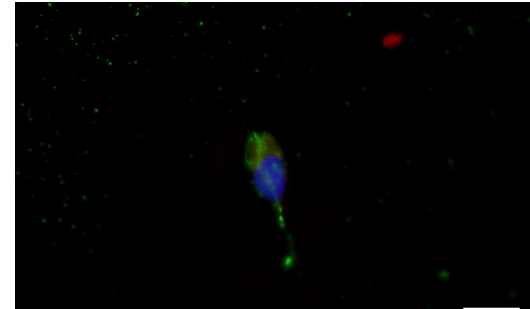


Figure 27: Immunostaining, cells with 100µM ERL

5 Discussion

5.1 Summary of results

In this study we investigated reendothelialization after implantation of BRS and DES in a preclinical animal model of early neoatherosclerosis. As previously shown in an animal model of early neoatherosclerosis, a higher incidence of neoatherosclerosis was observed in DES compared with BRS (Nicol et al. 2020a). In work presented here, DES showed a significant lower rate of endothelialization above the stent struts 28 days after implantation compared to the magnesium-based BRS. Additionally, the effects of everolimus on the endothelial cell cultures were investigated: endothelial cells incubated with ERL showed an increased permeability for fluorescently labelled ac-LDL, due to an impaired endothelial barrier function and a decreased expression of VE-cadherin, as observed in the immunostaining of the cells.

5.2 Choice of animal models

Already several hundred years before Christ animals have been used for research. (Hajar 2011). In recent years criticism on the ethics of animal testing has led to the development of the concept of the 3R: replacement, reduction, refinement. The idea is to reduce the number of animals to the necessary minimum, refine the use of animals to lessen the pain and burden during the testing and to replace the usage of animals with lower organisms or alternative methods (Doke and Dhawale 2015; Hajar 2011). It's an approach to maintain the scientific progress, while finding ways to meet the critic's demands and strengthen the moral conscience.

5.2.1 Rabbit model

To find the right animal for an atherogenic investigation, the animals should have a similar lipid metabolism and resemble the pathophysiology of the human cardiovascular system. The investigated disease should develop in the same steps it does in human (e.g. same atherosclerotic lesions). In addition, the chosen animal should be easily available at a rational price and have a suitable size for the intended experiments (Fan et al. 2014).

The rabbit model for atherosclerosis is one of the most appropriate models to use for investigations of atherosclerotic disease and is often used. Since 2000, the numbers

of rabbits used for atherosclerotic research is declining, which might be affiliated to the introduction of mice models, which are easy to genetically modify. However, rodents such as mice and rats are phylogenetically farer away to humans than rabbits. While in human and rabbits the major plasma lipoprotein is LDL, the predominant one in mice and rats is HDL. Moreover rabbits have a low excretion of bile acid and react sensitive to cholesterol diet such as humans, whereas mice have a high excretion of bile acid and are resistant to a cholesterol diet (Fan et al. 2014). Hence, depending on the scientific issue it should be considered individually which one of the possible models fits best.

In our translational study the rabbit represents the most proper animal due to the cholesterol sensitivity that allows a fast process of atherosclerotic lesions and the size of the iliac arteries that fit human stents and catheters. Pigs also represent a frequently used model for the investigation of stents and atherosclerosis. Previous studies focusing on the reendothelialization after stent implantation preferred rabbits for that purpose (Waksman et al. 2017; Joner et al. 2008; Koppa et al. 2015). The reendothelialization is slower in rabbits than in pigs making it a more similar model to the human, even though both animals show faster endothelial regrowth (Finn et al. 2007b; Joner et al. 2008).

Additionally, other studies from our team investigated the accordance of the presentation of early neoatherosclerotic changes in rabbits with the ones in humans. The results showed that the rabbit is a suitable model for investigating the pathophysiology of neoatherosclerosis (Guo L. et al 2015).

5.3 Clinical challenges of BRS

Stent implantation is one of the most frequently performed intervention for obstructive coronary artery disease. While bare metal stents (BMS) and first-generation drug eluting stents (1G-DES) were limited by high rates of restenosis and stent thrombosis, the introduction of second generation drug eluting stents (2G-DES) could diminish the rate of long-term device failure . Even though the incidence of stent thrombosis with 2G-DES is low (approximately 0.4%), its high mortality (30-45%) makes it an important issue for the interventional community and for patients undergoing stent implantation and scientific efforts to better comprehend and further minimize such catastrophic events are highly necessary. With the introduction of bioresorbable vascular scaffolds,

the ongoing stimulus of a foreign, persistent body in the vascular artery wall could be avoided. In theory, fully degradable scaffolds would re-establish normal blood flow and vessel physiology and avert problems like stent thrombosis. However, studies on the clinical outcome of one of the first FDA approved and highly investigated Absorb BVS did not show superiority of BRS compared to DES. In contrast, a higher rate of target lesion failure was found in the BVS compared to a drug eluting stent with a higher number of target vessel myocardial infarction and device thrombosis (Kereiakes et al. 2017; Sotomi et al. 2017). Reasons for these failures were suboptimal implantation technique, malapposition during the dismantling process, neoatherosclerosis and thick struts that foster thrombogenic changes (Pradhan et al. 2019, Ortega-Paz et al. 2018, Yamaji et al. 2017).

Both devices, DES and BRS, face the problem of late device thrombosis. An important cause for late-term device failures in both DES and BRS represents the formation of neoatherosclerotic changes in the neointima (Adriaenssens et al. 2017; Kraak et al. 2018). Studies investigating the incidence of neoatherosclerosis in BMS and DES showed a lower rate of neoatherosclerosis in the BMS. In comparison to DES, BMS show a more rapid endothelialization. This lead to the hypothesis that delayed arterial healing in DES, seen as an incomplete reendothelialization of the stent struts, might play a crucial role in the genesis of neoatherosclerosis in DES (Nakazawa et al. 2011). In a former preclinical animal study investigating the appearance of early neoatherosclerotic lesions, magnesium-based BRS showed a lower incidence of neoatherosclerosis compared to DES (Nicol et al. 2020a). Hypothesizing that the endothelium plays a role in the development of neoatherosclerosis, the aim of this study was to investigate the endothelialization above the stent struts between BRS and DES 28 days after stent implantation. Our results showed a lower endothelialization above the stent struts in the vessels treated with a DES (42% in DES vs 92% in BRS, $p < 0,0001$) compatible with the idea that the impaired barrier function of the endothelium leads to a higher incidence of neoatherosclerosis in DES.

5.3.1 Previous investigations on reendothelialization

Otsuka et al compared the strut coverage of the Absorb BVS and the Xience DES in a healthy porcine coronary artery model 28 days after implantation. The results showed a complete strut coverage in both devices at this time point.

Another study comparing the endothelialization of a DES and the Absorb BRS in a healthy rabbit model showed diverse results. They compared an EES with a strut thickness of 74 μ m and a biodegradable PLGA copolymer abluminal coating, with a bioresorbable EES (bEES, Absorb BVS) with a strut thickness of 150 μ m and a circumferential coating with biodegradable PDLLA polymer. The results showed a greater endothelial coverage above the EES struts (87,5 % coverage) compared to the bEES (12,4 % coverage, $p=0.15$) (Koppara et al. 2015).

Waksman et al compared the endothelialization of the BRS Magmaris with the Absorb BVS after 28 days using a rabbit model. While the Absorb BVS has a thickness and width of 150/180 μ m and a Poly-DL-lactic acid (PDLLA) coating, the Magmaris has a thickness and width of 150/150 μ m, a biocompatible polylactic-acid (PLLA) coating and has hemodynamically beneficial round strut edges. After 28 days, the Magmaris showed a greater endothelial coverage than the Absorb (51,7% coverage above struts vs 19,3%, $p=0.0039$).

5.3.2 Factors influencing reendothelialization

Many factors in the study design regarding animal model and device factors might have an influence on the different outcomes of these previous works concerning the endothelialization over the stent struts of different devices

5.3.2.1 Animal model

Firstly, the reendothelialization largely depends on the animal species and the tissue conditions of either a healthy or a diseased model. Different to our study with an atherosclerotic rabbit model, Otsuka et al used a healthy porcine coronary artery model. The healing process in swine, likewise the reendothelialization, is faster in pigs than in rabbits and human, which may explain the observed complete coverage after 28 days in both devices (Finn et al. 2007b; Joner et al. 2008).

5.3.2.2 Stent geometry and coatings

Another factor that influences the endothelialization is the geometry and the coating of the device. Koppara et al observed a lower endothelialization of the BRS compared to the DES, whereas in our study the BRS showed a higher endothelialization than the DES. In the study from Koppara et al, the BRS had thicker stent struts than the DES and a different polymer to elute the drug, whereas we used devices with the exact

same strut geometry and coating. They observed a lower endothelialization over the BRS with the thicker struts (Koppara et al. 2015). One explanation for these differences to our findings could be related to the strut thickness and stent coatings. Stent geometry has an impact on the luminal flow conditions. Thicker struts disturb the luminal flow more than thinner ones (Kolandaivelu et al. 2011). These alterations result in different shear stress distributions over the stent surfaces. The low flow velocity caused by the fluid separation on the stent struts leads to an inhibition of the reendothelialization of the surfaces of the struts and the vessel (Chaabane et al. 2013). Furthermore, thicker stent struts increase platelet deposition, fibrin deposition and thrombin activation, representing a nidus for thrombosis (Kolandaivelu et al. 2011).

The results from the study of Waksman et al strengthens the hypothesis that different stent designs and coatings have an influence on the flow dynamics and therefore on the thrombogenicity and endothelialization. In their work, the Absorb BVS with a thickness and width of 150/180µm and a Poly-DL-lactic acid (PDLLA) coating showed a lower endothelialization than the Magmaris with a thickness and width of 150/150µm, a biocompatible polylactic-acid (PLLA) coating and hemodynamically beneficial round strut edges (Waksman et al. 2017).

5.3.2.3 Backbone material

In our study, influencing factors, such as different stent geometry and coatings were diminished: both devices elute the same amount of antiproliferative drugs, have the same drug-coating and the exact same stent geometry, leaving open the question, why endothelialization is enhanced in the Magmaris compared to the DES. Presumably, the difference in backbone material (magnesium versus stainless steel) could be causative for this difference in reendothelialization, as both devices used in this study were similar in all other aspects (= drug-type and -concentration, strut thickness and polymer-coating). In an in vitro experiment it was shown that the proliferation of endothelial cells is stimulated when incubating the cells with magnesium chloride (Sternberg et al. 2012). This would contribute to the hypothesis that the magnesium based BRS leads to a faster reendothelialization than the DES. Furthermore, studies described an antithrombotic effect of magnesium, presenting another advantage of magnesium based devices (Rukshin et al. 2002; Rapetto and Leoncini 2017). The exact mechanism why the reendothelialization is faster in the Magmaris than in DES remains unknown so far.

5.4 Effect of everolimus on the endothelium

In this study, we furthermore investigated the effect of everolimus on the endothelium and the cell-cell junctions, to underpin the hypothesis that an impaired endothelium is a key factor for atherogenic changes. The idea for the use of antiproliferative drugs is to prevent neointimal hyperplasia by reducing the proliferation of SMCs. However, while not specifically targeting SMCs, everolimus also has an effect on the proliferation of endothelial cells (Chaabane et al. 2013). The results of our in vitro experiments showed the impairment of the endothelial barrier by the antiproliferative drug, by increasing the permeability via destruction of the cells and the cell-cell junctions. More LDL could pass through the endothelial layer and might promote atherosclerotic changes. In another recent study of our work group, increased LDL passage led to the formation of foam cells when adding monocytes to the transwell experimental set-up (Nicol et al. 2020b). In other studies the increase in permeability of the endothelium after incubating with –limus drugs could also be shown. For example, Oroszlan et al described an increased permeability of the endothelium, seen as an increased passage of FITC-Dextran, after incubating the cells with a concentration of 100nM ERL. The authors hypothesized that the drugs increase the oxidative stress and thereby impair the cell-cell junctions (Oroszlán et al. 2008). In another study, Habib et al also described an increased passage of FITC-Dextran through the endothelial monolayer after incubation with Sirolimus (Habib et al. 2013).

6 Conclusion

The results of our study combined with the higher appearance of neoatherosclerotic lesions in DES may show the connection of the impaired endothelial coverage with damaged cell-cell junctions to the genesis of neoatherosclerotic lesions. Certainly, other factors might influence the changes in the neointima like the vascular inflammation after stent implantation. The local inflammation has an effect on the SMC proliferation and disposal of ECM, which can lead to atherosclerotic changes (Inoue et al. 2011). Other factors that influence the emergence of neoatherosclerosis are patient characteristics like comorbidity, drug tolerance and smoking (Yonetsu et al. 2012). Still, further studies are necessary to determine the underlying mechanisms and processes of neoatherosclerosis.

7 Limitations

In the first place, animal and cell culture studies can never represent the entirety of a human disease. With a diseased animal model an approximation is strived for, but it stays difficult to interpret the findings and transfer of results to humans has to be done with great caution. Furthermore, the methods used can never guarantee precision. For the investigation of the endothelialization of the stent struts, SEM was used. The analysis of a 3D vessel captured on a 2D picture surely distorts the measurement. Additionally, the analysis of the fluorescently marked ac-LDL particles using a plate reader-spectrophotometer in fluorescent mode is error prone. The current study should give an insight into the role of the endothelium and it's possible key role in the genesis of neoatherosclerosis, but further studies and clinical trials are needed to validate these findings.

8 Summary

Percutaneous coronary intervention has been established as an important therapy of coronary artery disease. With the evolution of stent technology and development of drug-eluting stents, the problem of device failures seen with early devices could be reduced drastically. However, a new manifestation of atherosclerosis in the stented area was discovered recently: neoatherosclerosis. The underlying pathomechanism is still not completely understood, but there is hypothesis that the endothelium might play a key role in the pathogenesis. An impaired endothelial barrier might lead to an increased passage of lipids and inflammatory cells promoting the formation of neoatherosclerotic changes.

In this study we investigated the pathophysiologic pathway of neoatherosclerosis with a focus on the reendothelialization of the stent struts. For this purpose we compared the strut surfaces of a bioresorbable scaffold (Magmaris, Biotronik AG) and a DES (316L SS-DES, Biotronik AG) 28 days after implantation in the iliac arteries of 12 New Zealand White Rabbits using scanning electron microscopy. Both devices had the identical device geometry and drug release rate. Furthermore, we investigated the effect of everolimus on the endothelium. Therefore, we used a transwell model, to analyse the permeability of a HUVEC monolayer incubated with different concentrations of ERL, and performed an immunostaining of the cell-cell junctions. The results of the in vivo experiment showed significantly less endothelialization of the stent struts in DES (42% endothelial coverage) compared to the BRS (91% endothelial coverage). The in vitro permeability assay showed an increased passage of ac-LDL when incubated with ERL and less VE-cadherin in the immunostaining.

Given the results of our previous study that showed a higher incidence of neoatherosclerosis in DES than in BRS, our results support the concept of impaired endothelialization to the development of neoatherosclerosis, leading to an increased migration of LDL into the subendothelium. Therefore, magnesium-based BRS might represent an attractive alternative to DES by providing an improved long-term safety profile. Yet, further studies are needed to determine the clinical significance of our findings.

9 List of references

Adriaenssens, Tom; Joner, Michael; Godschalk, Thea C.; Malik, Nikesh; Alfonso, Fernando; Xhepa, Erion et al. (2017): Optical Coherence Tomography Findings in Patients With Coronary Stent Thrombosis: A Report of the PRESTIGE Consortium (Prevention of Late Stent Thrombosis by an Interdisciplinary Global European Effort). In: *Circulation* 136 (11), S. 1007–1021. DOI: 10.1161/CIRCULATIONAHA.117.026788.

Aikawa, M.; Rabkin, E.; Sugiyama, S.; Voglic, S. J.; Fukumoto, Y.; Furukawa, Y. et al. (2001): An HMG-CoA reductase inhibitor, cerivastatin, suppresses growth of macrophages expressing matrix metalloproteinases and tissue factor in vivo and in vitro. In: *Circulation* 103 (2), S. 276–283. DOI: 10.1161/01.cir.103.2.276.

Airhart, S.; Murali, S. (2017): Ischemic Cardiomyopathy. In: Douglas B. Sawyer und Ramachandran S. Vasan (Hg.): *Encyclopedia of Cardiovascular Research and Medicine*. Saint Louis: Elsevier Science, S. 145–154.

Bavry, Anthony A.; Kumbhani, Dharam J.; Helton, Thomas J.; Borek, Przemyslaw P.; Mood, Girish R.; Bhatt, Deepak L. (2006): Late thrombosis of drug-eluting stents: a meta-analysis of randomized clinical trials. In: *The American journal of medicine* 119 (12), S. 1056–1061. DOI: 10.1016/j.amjmed.2006.01.023.

Bundesärztekammer; Kassenärztliche Bundesvereinigung (KBV); Arbeitsgemeinschaft der Wissenschaftlichen Medizinischen Fachgesellschaften (AWMF) (2016): *Nationale VersorgungsLeitlinie Chronische KHK - Langfassung*, 4. Auflage. Version 1.

Byrne, R. A.; Joner, M.; Kastrati, A. (2009): Polymer coatings and delayed arterial healing following drug-eluting stent implantation. In: *Minerva cardioangiologica* 57 (5), S. 567–584.

Byrne, Robert A.; Joner, Michael; Kastrati, Adnan (2015a): Stent thrombosis and restenosis: what have we learned and where are we going? The Andreas Grüntzig Lecture ESC 2014. In: *European heart journal* 36 (47), S. 3320–3331. DOI: 10.1093/eurheartj/ehv511.

Byrne, Robert A.; Serruys, Patrick W.; Baumbach, Andreas; Escaned, Javier; Fajadet, Jean; James, Stefan et al. (2015b): Report of a European Society of Cardiology-European Association of Percutaneous Cardiovascular Interventions task force on the evaluation of coronary stents in Europe: executive summary. In: *European heart journal* 36 (38), S. 2608–2620. DOI: 10.1093/eurheartj/ehv203.

Chaabane, Chiraz; Otsuka, Fumiyuki; Virmani, Renu; Bochaton-Piallat, Marie-Luce (2013): Biological responses in stented arteries. In: *Cardiovascular research* 99 (2), S. 353–363. DOI: 10.1093/cvr/cvt115.

Dietz; Rauch (2003): Leitlinie zur Diagnose und Behandlung der chronischen koronaren Herzerkrankung der Deutschen Gesellschaft für Kardiologie – Herz- und Kreislaufforschung (DGK). In: *Zeitschrift für Kardiologie, Band* 92 (6).

- Doke, Sonali K.; Dhawale, Shashikant C. (2015): Alternatives to animal testing: A review. In: *Saudi pharmaceutical journal : SPJ : the official publication of the Saudi Pharmaceutical Society* 23 (3), S. 223–229. DOI: 10.1016/j.jsps.2013.11.002.
- Fan, Jianglin; Kitajima, Shuji; Watanabe, Teruo; Xu, Jie; Zhang, Jifeng; Liu, Enqi; Chen, Y. Eugene (2014): Rabbit models for the study of human atherosclerosis: from pathophysiological mechanisms to translational medicine. In: *Pharmacology & therapeutics* 0, S. 104–119. DOI: 10.1016/j.pharmthera.2014.09.009.
- Finn, Alope V.; Joner, Michael; Nakazawa, Gaku; Kolodgie, Frank; Newell, John; John, Mike C. et al. (2007a): Pathological correlates of late drug-eluting stent thrombosis: strut coverage as a marker of endothelialization. In: *Circulation* 115 (18), S. 2435–2441. DOI: 10.1161/CIRCULATIONAHA.107.693739.
- Finn, Alope V.; Nakazawa, Gaku; Joner, Michael; Kolodgie, Frank D.; Mont, Erik K.; Gold, Herman K.; Virmani, Renu (2007b): Vascular responses to drug eluting stents: importance of delayed healing. In: *Arteriosclerosis, thrombosis, and vascular biology* 27 (7), S. 1500–1510. DOI: 10.1161/ATVBAHA.107.144220.
- Fishman et al. (1994): A Randomized Comparison of Coronary-Stent Placement and Balloon Angioplasty in the Treatment of Coronary Artery Disease. In: *The New England journal of medicine* (Vol.331 No.8), S. 496–501.
- Grüntzig, A.; Schneider, H. J. (1977): Die perkutane Dilatation chronischer Koronarstenosen--Experiment und Morphologie. In: *Schweizerische medizinische Wochenschrift* 107 (44), S. 1588.
- Grüntzig, A. R.; Senning, A.; Siegenthaler, W. E. (1979): Nonoperative dilatation of coronary-artery stenosis: percutaneous transluminal coronary angioplasty. In: *The New England journal of medicine* 301 (2), S. 61–68. DOI: 10.1056/NEJM197907123010201.
- Habib, Anwer; Karmali, Vinit; Polavarapu, Rohini; Akahori, Hirokuni; Cheng, Qi; Pachura, Kim et al. (2013): Sirolimus-FKBP12.6 impairs endothelial barrier function through protein kinase C- α activation and disruption of the p120-vascular endothelial cadherin interaction. In: *Arteriosclerosis, thrombosis, and vascular biology* 33 (10), S. 2425–2431. DOI: 10.1161/ATVBAHA.113.301659.
- Hajar, Rachel (2011): Animal testing and medicine. In: *Heart views : the official journal of the Gulf Heart Association* 12 (1), S. 42. DOI: 10.4103/1995-705X.81548.
- Haude, Michael; Ince, Hüseyin; Kische, Stephan; Abizaid, Alexandre; Tölg, Ralph; Alves Lemos, Pedro et al. (2018): Safety and clinical performance of a drug eluting absorbable metal scaffold in the treatment of subjects with de novo lesions in native coronary arteries: Pooled 12-month outcomes of BIOSOLVE-II and BIOSOLVE-III. In: *Catheterization and cardiovascular interventions : official journal of the Society for Cardiac Angiography & Interventions* 92 (7), E502-E511. DOI: 10.1002/ccd.27680.
- Herold, Gerd (Hg.) (2018): Innere Medizin 2018. Eine vorlesungsorientierte Darstellung : unter Berücksichtigung des Gegenstandskataloges für die Ärztliche Prüfung : mit ICD 10-Schlüssel im Text und Stichwortverzeichnis. Dr. Gerd Herold. Köln: Gerd Herold.

- Holmes, David R.; Kereiakes, Dean J.; Garg, Scot; Serruys, Patrick W.; Dehmer, Gregory J.; Ellis, Stephen G. et al. (2010): Stent thrombosis. In: *Journal of the American College of Cardiology* 56 (17), S. 1357–1365. DOI: 10.1016/j.jacc.2010.07.016.
- Inoue, Teruo; Croce, Kevin; Morooka, Toshifumi; Sakuma, Masashi; Node, Koichi; Simon, Daniel I. (2011): Vascular Inflammation and Repair: Implications for Reendothelialization, Restenosis, and Stent Thrombosis. In: *Jacc. Cardiovascular Interventions* 4 (10), S. 1057–1066. DOI: 10.1016/j.jcin.2011.05.025.
- Joner, Michael; Finn, Alope V.; Farb, Andrew; Mont, Erik K.; Kolodgie, Frank D.; Ladich, Elena et al. (2006): Pathology of drug-eluting stents in humans: delayed healing and late thrombotic risk. In: *Journal of the American College of Cardiology* 48 (1), S. 193–202. DOI: 10.1016/j.jacc.2006.03.042.
- Joner, Michael; Nakazawa, Gaku; Finn, Alope V.; Quee, Shawn Chin; Coleman, Leslie; Acampado, Eduardo et al. (2008): Endothelial cell recovery between comparator polymer-based drug-eluting stents. In: *Journal of the American College of Cardiology* 52 (5), S. 333–342. DOI: 10.1016/j.jacc.2008.04.030.
- Kereiakes, Dean J.; Ellis, Stephen G.; Metzger, Christopher; Caputo, Ronald P.; Rizik, David G.; Teirstein, Paul S. et al. (2017): 3-Year Clinical Outcomes With Everolimus-Eluting Bioresorbable Coronary Scaffolds: The ABSORB III Trial. In: *Journal of the American College of Cardiology* 70 (23), S. 2852–2862. DOI: 10.1016/j.jacc.2017.10.010.
- Knuuti, Juhani; Wijns, William; Saraste, Antti; Capodanno, Davide; Barbato, Emanuele; Funck-Brentano, Christian et al. (2020): 2019 ESC Guidelines for the diagnosis and management of chronic coronary syndromes. In: *European heart journal* 41 (3), S. 407–477. DOI: 10.1093/eurheartj/ehz425.
- Kolandaivelu, Kumaran; Swaminathan, Rajesh; Gibson, William J.; Kolachalama, Vijaya B.; Nguyen-Ehrenreich, Kim-Lien; Giddings, Virginia L. et al. (2011): Stent thrombogenicity early in high-risk interventional settings is driven by stent design and deployment and protected by polymer-drug coatings. In: *Circulation* 123 (13), S. 1400–1409. DOI: 10.1161/CIRCULATIONAHA.110.003210.
- Koppara, Tobias; Cheng, Qi; Yahagi, Kazuyuki; Mori, Hiroyoshi; Sanchez, Oscar David; Feygin, Julia et al. (2015): Thrombogenicity and early vascular healing response in metallic biodegradable polymer-based and fully bioabsorbable drug-eluting stents. In: *Circulation. Cardiovascular interventions* 8 (6), e002427. DOI: 10.1161/CIRCINTERVENTIONS.115.002427.
- Kraak, Robin P.; Kajita, Alexandre H.; Garcia-Garcia, Hector M.; Henriques, Jose P. S.; Piek, Jan J.; Arkenbout, E. Karin et al. (2018): Scaffold thrombosis following implantation of the ABSORB BVS in routine clinical practice: Insight into possible mechanisms from optical coherence tomography. In: *Catheterization and cardiovascular interventions : official journal of the Society for Cardiac Angiography & Interventions* 92 (2), E106-E114. DOI: 10.1002/ccd.27475.
- Lüllmann-Rauch, Renate (2012): Taschenlehrbuch Histologie. 10 Tabellen. 4., vollst. überarb. Aufl. Stuttgart: Thieme.

Moriyama, Noriaki; Shishido, Koki; Tanaka, Yutaka; Yokota, Shohei; Hayashi, Takahiro; Miyashita, Hirokazu et al. (2018): Neoatherosclerosis 5 Years After Bioresorbable Vascular Scaffold Implantation. In: *Journal of the American College of Cardiology* 71 (17), S. 1882–1893. DOI: 10.1016/j.jacc.2018.02.051.

Nabel, Braunwald (2012): A Tale of Coronary Artery Disease and Myocardial Infarction. In: *N Engl J Med* 366 (10), S. 970. DOI: 10.1056/NEJMx120007.

Nakazawa, Gaku; Otsuka, Fumiyuki; Nakano, Masataka; Vorpahl, Marc; Yazdani, Saami K.; Ladich, Elena et al. (2011): The pathology of neoatherosclerosis in human coronary implants bare-metal and drug-eluting stents. In: *Journal of the American College of Cardiology* 57 (11), S. 1314–1322. DOI: 10.1016/j.jacc.2011.01.011.

Nef, H. M.; Abdel-Wahab, M.; Achenbach, S.; Joner, M.; Levenson, B.; Mehilli, J. et al. (2018): Medikamentenfreisetzende Koronarstents/-scaffolds und medikamentenbeschichtete Ballonkatheter. In: *Kardiologie* 12 (1), S. 26–52. DOI: 10.1007/s12181-017-0202-9.

Nicol, Philipp; Bulin, Anna; Castellanos, Maria Isabel; Stöger, Magdalena; Obermeier, Simone; Lewerich, Jonas et al. (2020a): Preclinical investigation of neoatherosclerosis in magnesium-based bioresorbable scaffolds versus thick-strut drug-eluting stents. In: *EuroIntervention : journal of EuroPCR in collaboration with the Working Group on Interventional Cardiology of the European Society of Cardiology*. DOI: 10.4244/EIJ-D-19-00747.

Nicol, Philipp; Lutter, Christoph; Bulin, Anna; Castellanos, Maria Isabel; Lenz, Tobias; Hoppmann, Petra et al. (2020b): Assessment of a pro-healing stent in an animal model of early neoatherosclerosis. In: *Scientific reports* 10 (1), S. 8227. DOI: 10.1038/s41598-020-64940-2.

Oroszlán, Melinda; Bieri, Michael; Ligeti, Nathalie; Farkas, Aniko; Koestner, Simon C.; Meier, Bernhard; Mohacsi, Paul J. (2008): Proliferation signal inhibitor-induced decrease of vascular endothelial cadherin expression and increase of endothelial permeability in vitro are prevented by an anti-oxidant. In: *The Journal of heart and lung transplantation : the official publication of the International Society for Heart Transplantation* 27 (12), S. 1311–1318. DOI: 10.1016/j.healun.2008.08.013.

Ortega-Paz, Luis; Brugaletta, Salvatore; Sabaté, Manel (2018): Impact of PSP Technique on Clinical Outcomes Following Bioresorbable Scaffolds Implantation. In: *Journal of clinical medicine* 7 (2). DOI: 10.3390/jcm7020027.

Otsuka, Fumiyuki; Byrne, Robert A.; Yahagi, Kazuyuki; Mori, Hiroyoshi; Ladich, Elena; Fowler, David R. et al. (2015): Neoatherosclerosis: overview of histopathologic findings and implications for intravascular imaging assessment. In: *European heart journal* 36 (32), S. 2147–2159. DOI: 10.1093/eurheartj/ehv205.

Otsuka, Fumiyuki; Finn, Alope V.; Yazdani, Saami K.; Nakano, Masataka; Kolodgie, Frank D.; Virmani, Renu (2012): The importance of the endothelium in atherothrombosis and coronary stenting. In: *Nature reviews. Cardiology* 9 (8), S. 439–453. DOI: 10.1038/nrcardio.2012.64.

Otsuka, Fumiyouki; Joner, Michael; Prati, Francesco; Virmani, Renu; Narula, Jagat (2014): Clinical classification of plaque morphology in coronary disease. In: *Nature reviews. Cardiology* 11 (7), S. 379–389. DOI: 10.1038/nrcardio.2014.62.

Pradhan, Akshyaya; Vishwakarma, Pravesh; Vankar, Sameer; Sethi, Rishi (2019): "The Unpredictable ABSORB" - Very Late Stent Thrombosis of Bioresorbable Vascular Scaffold. In: *Heart views : the official journal of the Gulf Heart Association* 20 (2), S. 65–69. DOI: 10.4103/HEARTVIEWS.HEARTVIEWS_18_19.

Rapetto, Claudio; Leoncini, Massimo (2017): Magmaris: a new generation metallic sirolimus-eluting fully bioresorbable scaffold: present status and future perspectives. In: *Journal of Thoracic Disease* 9 (Suppl 9), S903-13. DOI: 10.21037/jtd.2017.06.34.

Ross, R. (1999): Atherosclerosis--an inflammatory disease. In: *The New England journal of medicine* 340 (2), S. 115–126. DOI: 10.1056/NEJM199901143400207.

Ross, R.; Glomset, J.; Harker, L. (1977): Response to injury and atherogenesis. In: *The American Journal of Pathology* 86 (3), S. 675–684.

Rukshin, Vladimir; Shah, Prediman K.; Cercek, Bojan; Finkelstein, Ariel; Tsang, Vivian; Kaul, Sanjay (2002): Comparative antithrombotic effects of magnesium sulfate and the platelet glycoprotein IIb/IIIa inhibitors tirofiban and eptifibatide in a canine model of stent thrombosis. In: *Circulation* 105 (16), S. 1970–1975.

Serruys, Patrick W.; Garcia-Garcia, Hector M.; Onuma, Yoshinobu (2012): From metallic cages to transient bioresorbable scaffolds: change in paradigm of coronary revascularization in the upcoming decade? In: *European heart journal* 33 (1), 16-25b. DOI: 10.1093/eurheartj/ehr384.

Sigwart, U.; Puel, J.; Mirkovitch, V.; Joffre, F.; Kappenberger, L. (1987): Intravascular stents to prevent occlusion and restenosis after transluminal angioplasty. In: *The New England journal of medicine* 316 (12), S. 701–706. DOI: 10.1056/NEJM198703193161201.

Sotomi, Yohei; Onuma, Yoshinobu; Collet, Carlos; Tenekecioglu, Erhan; Virmani, Renu; Kleiman, Neal S.; Serruys, Patrick W. (2017): Bioresorbable Scaffold: The Emerging Reality and Future Directions. In: *Circulation research* 120 (8), S. 1341–1352. DOI: 10.1161/CIRCRESAHA.117.310275.

Sternberg, Katrin; Gratz, Matthias; Koeck, Kathleen; Mostertz, Joerg; Begunk, Robert; Loebler, Marian et al. (2012): Magnesium used in bioabsorbable stents controls smooth muscle cell proliferation and stimulates endothelial cells in vitro. In: *Journal of biomedical materials research. Part B, Applied biomaterials* 100 (1), S. 41–50. DOI: 10.1002/jbm.b.31918.

Taniwaki, Masanori; Radu, Maria D.; Zaugg, Serge; Amabile, Nicolas; Garcia-Garcia, Hector M.; Yamaji, Kyohei et al. (2016): Mechanisms of Very Late Drug-Eluting Stent Thrombosis Assessed by Optical Coherence Tomography. In: *Circulation* 133 (7), S. 650–660. DOI: 10.1161/CIRCULATIONAHA.115.019071.

Thanassoulis, Afshar (2017): Atherosklerose - Herz-Kreislauf-Krankheiten - MSD Manual Profi-Ausgabe. Online verfügbar unter https://www.msdmanuals.com/de-de/profi/herz-kreislauf-krankheiten/arteriosklerose/atherosklerose#v31786549_de, zuletzt aktualisiert am 20.10.2020.000Z, zuletzt geprüft am 20.10.2020.261Z.

Virmani, R.; Kolodgie, F. D.; Farb, A.; Lafont, A. (2003): Drug eluting stents: are human and animal studies comparable? In: *Heart* 89 (2), S. 133–138.

Waksman, Ron; Zumstein, Philine; Pritsch, Martin; Wittchow, Eric; Haude, Michael; Lapointe-Corriveau, Capucine et al. (2017): Second-generation magnesium scaffold Magmaris: device design and preclinical evaluation in a porcine coronary artery model. In: *EuroIntervention : journal of EuroPCR in collaboration with the Working Group on Interventional Cardiology of the European Society of Cardiology* 13 (4), S. 440–449. DOI: 10.4244/EIJ-D-16-00915.

WHO (2018): Cardiovascular diseases (CVDs). Online verfügbar unter [http://www.who.int/news-room/fact-sheets/detail/cardiovascular-diseases-\(cvds\)](http://www.who.int/news-room/fact-sheets/detail/cardiovascular-diseases-(cvds)), zuletzt geprüft am 27.08.2018.

Wykrzykowska, Joanna J.; Kraak, Robin P.; Hofma, Sjoerd H.; van der Schaaf, Rene J.; Arkenbout, E. Karin; IJsselmuiden, Alexander J. et al. (2017): Bioresorbable Scaffolds versus Metallic Stents in Routine PCI. In: *The New England journal of medicine* 376 (24), S. 2319–2328. DOI: 10.1056/NEJMoa1614954.

Yahagi, Kazuyuki; Kolodgie, Frank D.; Otsuka, Fumiyuki; Finn, Alope V.; Davis, Harry R.; Joner, Michael; Virmani, Renu (2016): Pathophysiology of native coronary, vein graft, and in-stent atherosclerosis. In: *Nature reviews. Cardiology* 13 (2), S. 79–98. DOI: 10.1038/nrcardio.2015.164.

Yamaji, Kyohei; Ueki, Yasushi; Souteyrand, Geraud; Daemen, Joost; Wiebe, Jens; Nef, Holger et al. (2017): Mechanisms of Very Late Bioresorbable Scaffold Thrombosis: The INVEST Registry. In: *Journal of the American College of Cardiology* 70 (19), S. 2330–2344. DOI: 10.1016/j.jacc.2017.09.014.

Yonetsu, Taishi; Kato, Koji; Kim, Soo-Joong; Xing, Lei; Jia, Haibo; McNulty, Iris et al. (2012): Predictors for neoatherosclerosis: a retrospective observational study from the optical coherence tomography registry. In: *Circulation. Cardiovascular imaging* 5 (5), S. 660–666. DOI: 10.1161/CIRCIMAGING.112.976167.

10 List of figures

Figure 1: Classification of atherosclerotic lesions modified after Yahagi et al, 2016..	3
Figure 2: Timeline of animal experiment.....	13
Figure 3: exemplary marking of the measured area of strut 8 (white area) in half 1 of the DES from rabbit 48, for this example the picture was edited with paint (Paint, Microsoft Windows 1903)	20
Figure 4: exemplary marking of the measured area of strut 8 (white area) in half 2 of the DES from rabbit 48, for this example the picture was edited with paint (Paint, Microsoft Windows 1903)	20
Figure 5: exemplary marking of the measured of not endothelialized areas (white edging) in BRS from rabbit 43, for this example the picture was edited with paint (Paint, Microsoft Windows 1903)	21
Figure 6: setup of 24 well plate for preliminary experiment.....	23
Figure 7: schematic representation transwell model.....	24
Figure 8: setup of 12 well plate with different ERL concentrations for Permeability assay	25
Figure 9: 96 well plate for spectrophotometer analysis, yellow framed: known ac-LDL concentrations for standard curve, red framed: samples from the upper chamber of the permeability assay with ERL concentrations given, blue frame: samples from the lower chamber of the permeability assay with ERL concentrations given.....	26
Figure 10: SEM overview of a drug eluting stent	30
Figure 11: SEM overview of a bioresorbable scaffold.....	30
Figure 12: magnification from DES: uncovered struts	30
Figure 13: magnification from BRS: nearly total endothelialization	30
Figure 14: Endothelialization above stent struts, DES vs BRS.....	32
Figure 15: standard curve for LDL measurement, x-axis: ac-LDL concentration, y-axis: measurement of the plate reader in fluorescent mode	33
Figure 16: amount of ac-LDL that passed through the monolayer, results from one experiment.....	34
Figure 17: results n=3, Mean percentage of LDL that passed through the monolayer from all 3 experiments	35
Figure 18: trend line of mean percentage of LDL that passed through the monolayer, y-axis: ERL concentration 1=w/o, 2=10nM, 3=100nM, 4=1µM, 5=10µM, 6=100µM .	35
Figure 19: VE-cadherin staining of the cell-cell junctions, green	36

Figure 20: Phalloidin staining of cytoskeleton, red.....	36
Figure 21: Dapi staining of the nucleus, blue.....	36
Figure 22: Immunostaining, cells w/o ERL	37
Figure 23: Immunostaining, cells with 10nM ERL.....	37
Figure 24: Immunostaining, cells with 100nM ERL.....	37
Figure 25: Immunostaining, cells with 1 μ M ERL.....	37
Figure 26: Immunostaining, cells with 10 μ M ERL.....	37
Figure 27: Immunostaining, cells with 100 μ M ERL.....	37

11 List of tables

Table 1: Storage Protocol	17
Table 2: protocol for sample preparation.....	18
Table 3: Material for sample preparation (all material from the chemistry lab at the Max-Schaldach Stiftungsprofessur).....	18
Table 4: Contents of Endothelial Cell Growth Medium Supplement.....	22
Table 5: ERL stock solution	25
Table 6: ERL dilution.....	25
Table 7: LDL dilution	25
Table 8: LDL dilutions for standard curve.....	27
Table 9: Dilutions for Immunostaining	28
Table 10: results from the analysis of the samples	31
Table 11: measurements for the standard curve; X: ac-LDL concentration, Y: measurement from plate reader in fluorescent mode	33
Table 12: means of table 11 +/- standard deviation.....	32
Table 13: calculation table to evaluate the part of LDL that passed through the monolayer.....	34

12 List of abbreviations

ASS	acetylsalicylic acid
BMS	bare metal stent
BRS	bioresorbable scaffold
BVS	bioresorbable vascular scaffold
CABG	coronary artery bypass grafting
CAD	coronary artery disease
CCS	Canadian cardiovascular society
CPD	critical point dryer
CVD	cardiovascular disease
DAPI	4',6-diamidin-2-phenylindol
DAPT	dual antiplatelet therapy
DES	drug eluting stent
1G-DES	first generation drug eluting stent
2G-DES	second generation drug eluting stent
DMSO	dimethyl sulfoxide
EC	endothelial cell
EES	everolimus eluting stent
bEES	bioresorbable everolimus eluting stent
EMC	extra cellular matrix
ERL	everolimus
EtOH	ethanol
FDA	food and drug administration
HUVEC	human umbilical vein EC
i.v.	intravenous
NA	neoatherosclerosis
NYHA	New York Heart Association
OMT	optimal medical therapy
PBS	phosphate buffered saline
PCI	percutaneous coronary intervention

s.c.	subcutaneous
SEM	scanning electron microscopy
SMC	smooth muscle cell
SPB	sodium phosphate buffer
ST	stent thrombosis
TCFA	thin-cap fibroatheromas
VE-Cadherin	vascular endothelial cadherin
VLDL	very low-density lipoprotein
VLST	very late stent thrombosis

13 Attachments

13.1 Recording schedule for animal model

Aufzeichnungsplan TVA „Untersuchungen zu Entstehungsmechanismen und Therapieansätzen sowie Evaluierung neuartiger bildgebender Detektionsverfahren bei Neoatherosklerose am Kaninchenmodell“

Identifikationsnummer (Ohrtätowierung): _____

Herkunft des Tieres: _____

Datum Ankunft des Tieres: _____

Tier Studien-ID: _____

Projekt-AZ: _____

Unterschrift Projektleiter oder Stellvertreter: _____

Tierart/ Alter/Gewicht der Tiere	Gruppe: (Stent- Typ:DES/BRS)	Datum Beginn der Diät	Datum Euthanasie
NZW Kaninchen Gewicht Ankunft: Geschlecht: männl.	LIA: RIA:		
	1. Denudation + Stent-Implantation:		
	Datum:		
OP/Narkose- Verlauf			
Post operatives Befinden (innerhalb 2 Stunden)			
Post operative Analgesie (Art, Zeitraum, Dosierung)			
Probenentnahme nach Euthanasie			
Sonstiges			

Score Sheet zur Bewertung der auftretenden post operativen Belastung zum TVA „Untersuchungen zu Entstehungsmechanismen und Therapieansätzen sowie Evaluierung neuartiger bildgebender Detektionsverfahren bei Neoatherosklerose am Kaninchenmodell“

Projektleiter: PD Dr. Baumgartner

Animal ID: Gruppe: Projekt-AZ:	Datum Versuchsbeginn:	Datum 1. Denudation + Stentimplantation:	Datum 2. Denudation:	Datum												
Untersucher:	Datum	Datum	Datum	Datum	Datum	Datum	Datum	Datum	Datum	Datum	Datum	Datum	Datum	Datum	Datum	Datum
Allgemein körperlicher Zustand																
Körpergewicht (0 = Gewichtsverlust <5%; 1 = Gewichtsverlust 5-10%; 2 = Gewichtsverlust 10-15%; 3 = Gewichtsverlust >15%)																
Futeraufnahme (0 = ja, Menge physiologisch; 1 = reduziert; 2 = keine)																
Tränkeaufnahme (0 = ja, Menge physiologisch; 1 = reduziert; 2 = keine)																
Kotabsatz (0= vorhanden; 1 = wenig; 2 =kein)																
Harnabsatz (0= vorhanden; 2 = kein)																
Aktivität (0= aktiv; 1 = wenig aktiv; 2 = inaktiv)																
Aufmerksamkeit (0= vorhanden; 1 = reduziert; 2 = stark reduziert; 3 = keine)																
Fell (0=gepflegt; 1 = leicht struppig; 2 =ungepflegt/struppig)																
Atmung (0=normal; 1= frequent; 2 = angestrengt/stridor)																
Schleimhäute (0= rosa; 1 = blassrosa; 2 = anämisch/zyanotisch/ikterisch)																
Anzeichen für Schmerz (0=keine; 1= gering; 2 = mittelgradig; 3 = hochgradig)																
Zusätzliche Untersuchung																
Palpation der Hinterfüße (0= keine Anzeichen auf Veränderung; 2 = schwacher Femoralispuls; 3 = kalte Pfoten oder Ödematisierung /Blaufärbung der Zehen bzw. des Krallenbets / Automutilation)																

13.3 Score sheet

Lahmheit der Hintergliedmaßen (0= keine Lahmheit; 3 = Lahmheit)																			
Adspektion/Palpation des Halses (0= normal Wundheilung; 1 = leichtes Hämatom; 2 = mittelgradiges Hämatom/Schwellung oder verzögerte Wundheilung verbunden mit Schmerzen; 3 = hochgradiges Hämatom oder starke Wundheilungsstörung verbunden mit starken Schmerzen)																			

Anmerkung zur Beurteilung: Das Opioid-Analgetikum Buprenorphin kann so sedierend wirken, dass das Allgemeinbefinden inkl. Futteraufnahme und Kotabsatz in dieser Wirkdauer etwas reduziert sein kann.

Kontrollrhythmus:

VOR dem Eingriff: alle 3 Tage

NACH dem Eingriff (Tag 7 bzw. Tag 63): 7 Tage nach OP täglich; danach alle 3 Tage

Einteilung der Belastung nach Erreichen eines Scores von:

Score 0: keine Belastung

Score 1: geringe Belastung → Tier bleibt im Versuch, Score-Frequenz mind. 1x täglich

Score 2: mäßige Belastung → Abklärung der Ursache durch tierärztliche Untersuchung; ggf. symptomatische Behandlung wie z.B. Schmerzbehandlung, Antibiose etc.

→ erneute Evaluierung des Score-Protokolls ca. 2 Std. nach erfolgreicher Behandlung

→ wenn keine Besserung der Symptome, Abbruch je nach Symptomatik nach spätestens 2 Tagen

Score 3: starke Belastung → Abbruch des Versuchs

Humaner Endpunkt, sofortiger Abbruch mit Euthanasie des Tieres:

- Score-Wert von 2 über 2 Tage
- Score-Wert von 3

13.4 Intervention protocol

Datum	Tierart	Geschlecht	KGW	Projekt-Nr.	Tiernummer	Durchführender
	Kaninchen	männlich				
Zeit						
Katheterintervention						
	HF					
	SpO2					
	EICO2					
	AF					
	Peak (cm H ₂ O)					
	l.v.-Zugang Ohrvene					
	Intubation					
	Präp- A. carotis communis					
	Angiographie					
	Denudation					
	Implantation Stent					
	Ligation A. carotis communis					
	Medikamente:					
	Propofol 1% (ml)					
	Propofol 2% (ml/h)					
	Heparin (150 I.E./kg)					
	Kontrastmittel					
	Fentanyl (ml)					
	Enrofloxacin (10 mg/kg) s.c.					
	Buprenorphin (0,01 mg/kg) s.c.					
Bemerkungen:						

14 Note of thanks

Firstly, I would like to thank my supervisor Prof Dr. med Michael Joner, who enabled me to do this doctoral thesis and was always there to help me and support me with advice.

Moreover, I would like to thank Dr. Johannes Fischer from the center for preclinical research and Prof. Dr. Robert Schmiedl from the department of expert future technologies – physics, future technologies & IP / vascular intervention / Biotronik SE & Co. KG, as well as all the members of our workgroup who accompanied me through this time.

Special thanks goes to Carina Lorenz and Anna Bulin who encouraged me during the animal study and beyond, Maria Isabel Castellanos who taught me everything I had to know for the cell culture and Dr. Philipp Nicol for his help throughout the whole project.

In addition, I would like to thank my parents Sigrid and Christian, my stepdad Sascha, my Brothers Julius and Maximilian, and my boyfriend Tobias, who were always there for me when I lost track or needed somebody to talk to. They never complained about my complaining.

Thank you all very much!